Numerical Investigations to Identify Environmental Factors for Field-Scale Reactive Transport of Pathogens at Riverbank Filtration Sites

Knabe, D.[1], Dwivedi, D.[2], Wang, H.[3], Griebler, C.[3], Engelhardt, I.[1]

[1] Technische Universität Berlin, Institute for Applied Geosciences, Department of Hydrogeology, Ernst-Reuter-Platz 1, 10587 Berlin, Germany

[2] Lawrence Berkeley National Laboratory, Earth and Environmental Sciences Area, Geochemistry Department, Berkeley, CA, USA

[3] University of Vienna, Department of Functional and Evolutionary Ecology, Division of Limnology, Djerassiplatz 1, 1030 Vienna, Austria

Corresponding author: Dustin Knabe (dustin.knabe@tu-berlin.de)

Keywords: bank filtration, transport modelling, virus, bacteria, pathogen, PFLOTRAN

Highlights/Key points:

- Travel time was the main factor for transport of coliforms and somatic coliphages
- Travel distance was the main factor for transport of adenovirus
- A changing colmation layer resulted in variable coliform removal
- Temperature and oxygen content had little impact on virus and bacteria transport

Abstract

While induced bank filtration is a proven method for facilitating sustainable drinking water production, it is at risk from surface water contaminations (e.g., pathogens). Induced bank filtration and pathogen transport in groundwater have been studied extensively. However, long-term studies that consider real-world conditions are missing. These conditions include seasonal changes to environmental conditions and waterworks operations. Therefore, to analyze the effect of seasonal changes on the transport of human pathogenic viruses and their indicators in induced bank filtration, concentrations of adenoviruses and pathogen indicators were monitored over 16 months at an active bank filtration plant at the Rhine River, in Düsseldorf (Germany). Based on this data, a 2D groundwater model was created in PFLOTRAN that simulated flow, heat transport, conservative transport of chloride and the resulting electrical conductivity, reactive transport of oxygen and nitrate, and colloid-based transport of coliforms, somatic coliphages, and adenoviruses. The results show that reduced travel time was the key factor determining periods with a low removal of coliforms and somatic coliphages in the aquifer. Travel time was controlled by river level variations during rainy seasons, and the waterworks extraction rates during dry seasons. For adenovirus transport, travel distance in the subsurface appeared to be the key factor, while travel time had no significant impact. Coliform removal increased when the colmation layer permeability decreased, while coliphage and adenovirus removal was unaffected by the colmation layer permeability. Seasonal changes in temperature and oxygen content did not significantly impact the removal of coliphages and adenoviruses in groundwater. Denitrifying conditions correlated with a lowered coliform removal, but the modelling could not establish a connection between denitrifying conditions and coliform removal. Our study showed that removal of pathogens and pathogen indicators at induced bank filtration plants varies greatly in time and space (e.g., for coliforms from 1 to 4 log-levels at 20 m travel distance), and that adenovirus transport differs considerably from transport of coliforms and somatic coliphages.

1. Introduction

Induced bank filtration (IBF), a type of managed aquifer recharge (MAR), is a proven method for facilitating sustainable drinking water production, especially in regions with limited groundwater resources but with large surface water bodies (Dillon et al., 2019). IBF is employed worldwide, often in urbanized regions (e.g., the city of Berlin and cities along the Danube and Rhine rivers in Europe) (Dillon et al., 2019; Gillefalk et al., 2018; Sprenger et al., 2017). For IBF, extraction wells are placed close to river or lake banks. Most of the extracted water originates from the surface water body, but has undergone a subsurface passage during which natural physical, chemical, and biological processes can reduce contaminant concentrations. However, in surface waters at riverbank filtration sites, various contaminants with different degradation behavior can be present (e.g., organic compounds, pharmaceuticals, metals, and human pathogens, such as viruses and bacteria) (Engelhardt et al., 2014; Farnsworth and Hering, 2011; Hu et al., 2016; Maeng et al., 2011; Sprenger et al., 2014). Additionally, the efficacy of IBF in reducing contaminant concentrations is subject to environmental and climatic conditions. For example, floods are typically assessed as impairing IBF performance because they shorten the travel times of contaminants (Sprenger et al., 2011).

Human pathogens are typically released into surface water with treated wastewater (Montazeri et al., 2015). Typical human pathogens in surface waters are adenovirus, rotavirus, *enterococcus*, and *Giardia intestinalis*, which cause a variety of enteric diseases (WHO, 2017). Modern drinking water guidelines and regulations, such as those from the WHO (2017) and the European Union (2020), use bacterial and viral indicators (e.g., *E. coli* and bacteriophages) to assess the potential contamination by pathogens. However, studies have shown that bacterial and bacteriophage indicators, as well as model viruses such as MS2 (often employed in laboratory studies owing to safety restrictions when using human pathogenic viruses), cannot adequately represent the characteristic transport behavior and fate of pathogenic viruses (Boehm et al., 2019; Pang et al., 2021). This highlights the need to study the transport of real pathogens in the environment.

Viruses and bacteria are transported in groundwater as bio-colloids due to their size (nm to low µm). Transport of bio-colloids in the subsurface is affected by various processes such as advection, dispersion, inactivation (loss of infectivity), decay (destruction of the particle), attachment to and detachment from solid surfaces, and straining (physical filtration) at small pore throats (Hunt & Johnson, 2017). Numerous studies have shown that a large number of factors can influence the transport of (bio-)colloids in groundwater. These factors include porosity, colloid size, water flow velocity, temperature, pH, surface charge of colloids and sediments, ionic strength, concentration of multivalent ions, and micro- and nanoscale roughness/heterogeneity of grain surfaces (Johnson et al., 2018; Messina et al., 2015; Sadeghi et al., 2013; Sasidharan et al., 2017; Torkzaban and Bradford, 2016; Tufenkji and Elimelech, 2004). However, comparisons between field observations and laboratory experiments conducted under similar conditions show that laboratory studies typically overestimate the removal of viruses and bacteria during underground passage (see Oudega et al. (2021) and references therein).

In contrast to the large number of laboratory studies, detailed studies at the field-scale that investigate (pathogenic) viruses and bacteria transport are less frequent. Furthermore, many studies have focused on indicators, rather than on pathogens directly, and on artificial injection experiments. Such experiments were performed, for example, by Oudega et al. (2021) with bacterial endospores and coliphages, by Hornstra et al. (2018) with bacteriophages under anoxic conditions, and by Kvitsand et al. (2015) with bacteriophages in an aquifer located in a cold climate (6° C). Induced or natural bank filtration was studied for example by Betancourt et al. (2014), Sprenger et al. (2014) and Weiss et al. (2005). Removal of naturally occurring viruses at a vertical infiltration site was studied by Morrison et al. (2020). However, detailed and long-term (multi-month) field studies on pathogen

transport are rare. Thus, Bradford & Harvey (2017) concluded in their review publication that field research is needed to improve our understanding of virus and bacteria transport in groundwater.

While laboratory-scale models can account for a huge number of complex processes (including the effects of nanoscale heterogeneity, as in Johnson et al. (2018)), models that investigate field-scale processes are typically constrained to simple first-order kinetics due to numerical limitations and uncertainty about subsurface properties. Therefore, currently available field-scale models only include inactivation, attachment, and detachment using colloid filtration theory for the attachment coefficient (e.g., Oudega et al. (2021)). Some researchers have used two-site models considering favorable and unfavorable attachment sites (Sasidharan et al., 2021; Kvitsand et al., 2015). Hornstra et al. (2018) also considered blocking (limitation of attachment sites), and Knabe et al. (2021) included straining. However, employing a more detailed process-based numerical modelling approach is less common. In general, at field-scale, currently published models are still insufficient, because many processes are neglected, and the impact of heterogeneity (Bradford and Harvey, 2017) and transient boundary conditions (Wang et al., 2020) is disregarded.

Therefore, a 16-month monitoring campaign was performed to improve our understanding of virus and bacteria transport in groundwater at field-scale, and under natural uncontrolled transient hydraulic and geochemical conditions. The campaign included high-resolution measurements of selected pathogens and their indicators along a transect of an IBF waterworks facility in Düsseldorf, Germany (Wang et al., 2022). This study investigated environmental factors that vary greatly between seasons (river level, oxygen content, temperature, and riverbed permeability). A model-based analysis was conducted to investigate the impact of these parameters on transport of coliforms, somatic coliphages, and adenovirus during IBF. The numerical code PFLOTRAN, a subsurface flow and reactive transport code, was used for this goal. PFLOTRAN has been used by many researchers, including Avasarala et al. (2017), Dwivedi et al. (2018b), Hammond et al. (2011), Knabe et al. (2021), and Navarre-Sitchler et al. (2013). PFLOTRAN was selected as modelling code because of its scalability on high performance computing clusters. PFLOTRAN allows for faster calculation times, and its open source code enables flexibility in the definition of rate equations, making it a good choice for modelling complex reactive transport systems. This study aimed to identify key parameters and processes for virus and bacteria transport in induced bank filtration. This study also investigated the differences between viruses and bacteria transport. Using an active IBF facility as a research site allows for the study of transport processes under real-world conditions, which increases the practical relevance and the transferability of the results to other IBF sites.

2. Methods

2.1 Investigated field site and sample collection

This study was conducted at an IBF site at the Rhine River in Düsseldorf, Germany (Waterworks "Flehe"). This site has been investigated in several previous studies (Knabe et al., 2021; Sharma et al., 2012; Schubert, 2002). To investigate the transport of viruses and bacteria during IBF, a 16-month sampling campaign was conducted from the end of 01/2018 to 05/2019. Water samples were collected every two to four weeks in the Rhine River and in observations wells built along a transect perpendicular to the river (Figure 1). Samples were analyzed onsite for standard physical-chemical parameters (O_2, pH, electrical conductivity (EC)), and in the laboratory for major anions/cations, and selected microbiological parameters (total coliforms, *Escherichia coli*, somatic coliphages, F+ coliphages, and adenovirus). For the production well (PW), only mixed samples were available that contained water from multiple production wells. Additionally, piezometric pressure heads and temperature were measured continuously (every 5 min) in selected observation wells using data loggers (pressure-temperature (PT) logger: Solinst Levelogger Edge, temperature (T) logger: Onset

Tidbit v2). For the wells equipped with a PT- and a T-logger, the T-logger was placed 0.5 m above the PT-logger, with both being inside the screened well section (1 m). River water samples were collected about 700 m downstream of the transect at a sampling point for river water used by local water authorities, which gathers water from above the riverbed by using a pumping system. River level and temperature were measured continuously by the local water authorities at a gauging station 12.7 km downstream.

The sampling procedure and the analytical methods are described in detail in Wang et al. (2022). In brief, to quantify *E. coli* and coliforms, the Colilert-18 assay (ISO 9308-2, 1990) was used, while coliphage numbers were assessed according to Binder (2013). Adenovirus was quantified by digital droplet-PCR following the guidelines of Huggett (2020).

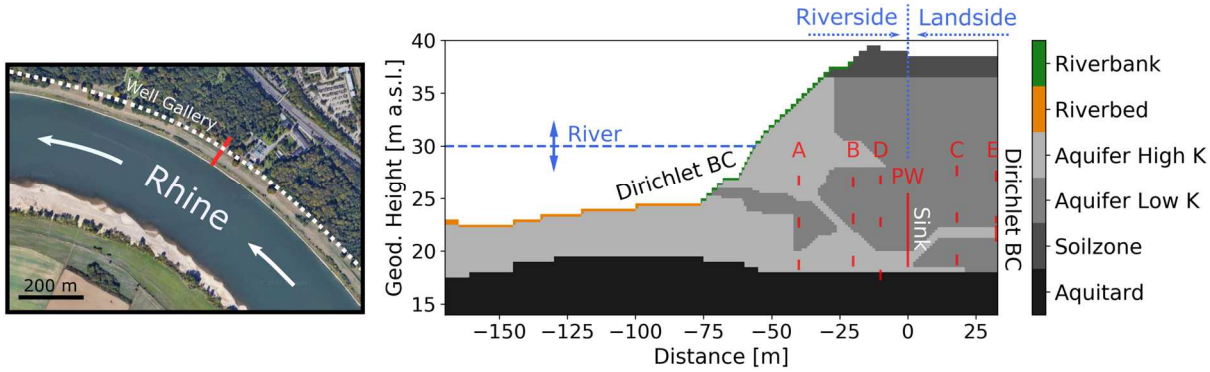

Figure 1. (Left) Top-down view of the site with the observation well transect in red. (Right) Modelled 2D transect with observation wells (A, B, C, D, E) and production well (PW) marked in red (lines mark the well screen positions), boundary conditions (BCs), and subsurface zones. Map data in left image from: Google, Imagery ©2022 AeroWest, Aerodata International Surveys, GeoBasis-DE/BKG, GeoContent, Maxar Technologies, Map data ©2022.

2.2 Numerical Model Setup – Flow, Transport, Discretization, Boundary Conditions

To simulate groundwater flow and transport of heat and solutes, as well as colloid-based transport of viruses and bacteria, the open-source modelling code PFLOTRAN was used (Hammond et al. (2014), www.pflotran.org). The TH (thermo-hydraulic) mode was employed for flow and heat transport; the GIRT (Global Implicit Reactive Transport) mode was employed for advective-dispersive and reactive transport. The rate equations described below were implemented via the Reaction-Sandbox feature.

The geometry and design of the production well gallery is such that the flow is perpendicular to the river and along the transect (Knabe et al., 2021; Schubert, 2002) (Figure 1, left). A numerical 2D model of the bank filtration transect (Figure 1, right) was set up using cells with dz = 0.25 m and a variable *dx* with finer discretization (square-shaped cells) in the riverbank to reduce numerical dispersion where flow is less horizontal:

$$dx = \begin{cases} 5.0\ m, x \in [-170, -165) \\ 2.0\ m, x \in [-165, -151) \\ 1.0\ m, x \in [-151, -80) \vee x \in [-46{,}33] \\ 0.5\ m, x \in [-80, -77) \vee x \in [-50, -46) \\ 0.25\ m, x \in [-77, -50) \end{cases}$$

Time-variant Dirichlet boundary conditions were set based on the measured data at the river and for the regional groundwater at Well Row E (Figure 1, right). The boundary conditions were set for piezometric pressure head, groundwater temperature, and concentrations of solutes, bacteria and viruses at two locations: (i) at the top of the cells adjacent to the river (green and orange in Figure 1,

right) and (ii) at the right-side boundary of the model domain. To account for the river level difference between the measuring point and transect location (12.7 km distance), the measured river level was corrected by using the known local average river level gradient of 0.2 m river level per 1000 m distance along the river. No-flow boundaries were set at the bottom (aquitard) and left side (flow to/from opposite riverbank was irrelevant). The production well (PW) was implemented as a sink located along the screened section.

The model simulates 500 days, starting at 01.01.2018 (Day 0) with a prior spin-up period of 50 days, with all boundary condition values set to those observed at Day 0 (except for all virus and bacteria species, whose concentrations were set to zero). This spin-up period provides the initial conditions for the piezometric pressure heads, temperature, and solute concentrations as quasi-steady state with the initial boundary condition values. PFLOTRAN's adaptive time stepping was used with at most 0.1-day time steps.

2.3 Subsurface Heterogeneity

Subsurface heterogeneity (Figure 1, right) was based on grain size analyses of the borehole profiles of the wells. The aquifer was divided into two zones — a highly permeable (HK), mostly coarse sand and gravel zone and a lower permeable (LK), higher medium sand content with some coarse sand and fine gravel zone — with two permeabilities K_{HK} and K_{LK}, and two porosities n_{HK} and n_{LK}, respectively. Permeability and porosity of the aquitard (silty fine sand) and the soil zone (silty clayey sand) were set to 10^{-11} m² and 0.2, respectively. The colmation layer (or clogging layer) directly at the interface between surface water and subsurface was discretized into an additional layer with a thickness of one cell (dz = 0.25 m). As a result of to numerical restrictions forced by the computational time, the previously published colmation layer thickness of 10 cm by Schubert (2002) had to be increased.

The (hydraulic) properties of the colmation layer can change over time due to (i) biogeochemical activity (bio-clogging, unclogging by grazing of benthic lifeforms), (ii) physical clogging by forced inflow of river water due to the constant pumping in the production wells, and (iii) changes in river discharge and sediment transport (Doppler et al., 2007; Engeler et al., 2011; Newcomer et al., 2016). The colmation layer was also divided into two zones: one located within the riverbed and the other zone located at higher elevation along the riverbank (Figure 1, right). The second zone was assumed to be strongly clogged because of the lower erosive potential of the river at this elevation and the presence of an armor layer to protect the riverbank.

This study compares two model concepts to consider the impact of the colmation layer: a time-invariant (TI) and a time-variant (TV) model. The TV model uses discrete time periods to account for changes in river level, extraction rates and a period when the waterworks pumps were shut down for 43 days for maintenance. The periods in the TV model were: (I) winter 2017/18 with a flood (days 0-40); (II) spring (days 40-100); (III) spring with maintenance period of the waterworks and including a 14-day recovery period after pumps were restarted (days 100-157); (IV) summer and autumn 2018 with falling river level (days 157-335); (V) winter 2018/19 with rising river level (days 335-425); (VI) end of winter 2018 and spring 2019 (days 425-500). The 14-day recovery in Period III is based on an older experiment mentioned in Schubert (2002) which indicated that reclogging took about 14 days. Permeabilities of the riverbed were calibrated for each period, the permeability of the riverbank was fixed at $K_{bank,clog} = 10^{-13}\ m^2$, except during Period III, where flow direction was reversed and unclogging is assumed to have occurred ($K_{bank,unclog} = 10^{-11}\ m^2$, $K_{bed,III} = 10^{-11}\ m^2$). For the TI model, both K_{bed} and K_{bank} were calibrated.

A single longitudinal dispersivity was set as a calibration parameter for all subsurface zones excluding the colmation layer ($\delta_{L,aq}$). Transversal dispersivity $\delta_{T,aq}$ was fixed at $\delta_{T,aq} = 0.1 \cdot \delta_{L,aq}$, similar to the approach by Hester et al. (2013). Dispersivity of the colmation layer and aquifer are unlikely to be similar, owing to different sediment structure and thus different heterogeneity. Initial model tests showed that dispersivity and porosity parameters for the colmation layer were highly uncertain after calibration with the conservative transport data. However, it was observed that a low dispersivity is needed for the colmation layer to potentially influence virus and bacteria transport. Because heterogeneity is reduced in the colmation layer a low dispersivity is reasonable. Therefore, longitudinal dispersivity and porosity for the colmation layer were fixed with $\delta_{L,colm} = 0.5\ m$ and $n_{colm} = 0.2$.

The thermal conductivity under saturated conditions for all layers was set to $\kappa = 3.3 \frac{W}{m \cdot K}$ while heat capacity of the aquifer layers was set to $c_{aqf} = 869 \frac{J}{kg \cdot K}$, since most of the sediments consist of sand and gravel. For the aquitard, it was set to $c_{naqf} = 1500 \frac{J}{kg \cdot K}$ to account for an increased fraction of fine clay and silt particles (Stauffer et al., 2013).

2.4 Mean Travel Time

Mean travel times were calculated with PFLOTRAN's "Tracer Mean Age" capability, which follows the method of Goode (1996) with the following equations (Gardner et al., 2015):

$$\frac{\partial A n \rho}{\partial t} = n\rho - \nabla \cdot A\rho q_w + \nabla \cdot n\rho D \cdot \nabla A + Q_A \quad (1)$$

$$A = \frac{\int_0^\infty tc\ dt}{\int_0^\infty c\ dt} \quad (2)$$

where A is the mean "age" for a mixture of groundwater [s], n is the porosity [-], ρ is the water density [kg m^{-3}], t is the time [s], c is the "concentration" of groundwater with a given age [mol L^{-1}], q_w is the groundwater flux [m³ s^{-1}], D is the dispersion coefficient [m² s^{-1}], and Q_A is a generic source/sink for age [kg m^{-3}]. The calculated water "age" was set to start at 0 days upon entering the model on either side (river or regional groundwater), and can therefore be interpreted as mean travel time from the model boundary at any observation point in the model domain.

2.5 Simulation of Aerobic Respiration and Denitrification

Consumption of oxygen by degradation of dissolved organic carbon (DOC, for simplicity assumed as acetate CH_3COO^-) was simulated according to previously published research (Knabe et al., 2021; Sharma et al., 2012). However, the equations were modified to allow a heterogeneous distribution of bacteria facilitating the reaction:

$$O_2 + \frac{1}{2} CH_3COO^- \rightarrow HCO_3^- + \frac{1}{2} H^+ \quad (3)$$

$$r_{O_2} = f_{T,O_2} \left[c_{b,O_2,j} \cdot k_{O_2} \cdot \left(\frac{c_{O_2}}{K_{O_2} + c_{O_2}} \right) \cdot \left(\frac{c_{DOC}}{K_{DOC,O_2} + c_{DOC}} \right) \right] \quad (4)$$

$$f_{T,O_2} = \frac{\exp\left(\beta_{O_2} \cdot T \cdot \left(1 - 0.5\frac{T}{T_{opt}}\right)\right)}{\exp\left(\beta_{O_2} \cdot 20°C \cdot \left(1 - 0.5\frac{20°C}{T_{opt}}\right)\right)} \quad (5)$$

where r_{O_2} is the reduction rate for O_2 [mol L^{-1} s^{-1}], $c_{O2/DOC}$ are the concentrations of O_2 and DOC respectively [mol L^{-1}], k_{O_2} is the rate constant [mol L^{-1} s^{-1}], K_{O_2} and K_{DOC,O_2} are Monod half saturation constants [mol L^{-1}], f_T is a factor including temperature effects on the reaction rate normalized to 20°C [-], T is temperature [°C], β_{O_2} is a calibration parameter influencing the rate of change for f_T with temperature [°C^{-1}], T_{opt} is the temperature at which the reaction rate is the fastest [°C], and $c_{b,O_2,j}$ is the normalized concentration of aerobic bacteria facilitating the reaction in zone j [-].

Aerobic bacteria were assumed to be immobile with a constant concentration. The subsurface was divided into two zones: the zone close to the river where more nutrients are available, resulting in higher aerobic bacteria concentrations ($c_{b,O_2,h}$= 1), and the zone in the bulk aquifer with lower aerobic bacteria concentrations ($c_{b,O_2,l}$ < 1, a calibration parameter). The extension of the zone with higher aerobic bacteria concentrations was adjusted during model calibration ($x_{aerobic}$, as horizontal and vertical distance from the river). Aerobic bacteria concentrations in model cells, where the zone border was located, were calculated as a weighted average between concentrations of both zones. The weights result from the proportion of the zones in the cell.

Denitrification was modelled similar to aerobic respiration, but includes an inhibition factor for dissolved oxygen (e.g., Arora et al., 2016; Dwivedi et al., 2018; Rodríguez-Escales et al., 2014):

$$NO_3^- + \frac{5}{8}CH_3COO^- + \frac{7}{2}H^+ \rightarrow \frac{1}{2}N_2 + \frac{5}{8}HCO_3^- + \frac{19}{8}H_2O \quad (6)$$

$$r_{NO_3^-} = f_{T,NO_3^-}\left[c_{b,NO_3^-,j} \cdot k_{NO_3^-} \cdot \left(\frac{c_{NO_3^-}}{K_{NO_3^-} + c_{NO_3^-}}\right) \cdot \left(\frac{c_{DOC}}{K_{DOC,N} + c_{DOC}}\right) \cdot \left(\frac{I_{O_2}}{I_{O_2} + c_{O_2}}\right)\right] \quad (7)$$

$$f_{T,NO_3} = \frac{\exp\left(\beta_{NO_3^-} \cdot T \cdot \left(1 - 0.5\frac{T}{T_{opt}}\right)\right)}{\exp\left(\beta_{NO_3^-} \cdot 20°C \cdot \left(1 - 0.5\frac{20°C}{T_{opt}}\right)\right)} \quad (8)$$

where $r_{NO_3^-}$ is the reduction rate for NO_3^- [mol L^{-1} s^{-1}], $c_{NO_3^-/O_2/DOC}$ is the concentration of NO_3^-, O_2 and DOC respectively [mol L^{-1}], $k_{NO_3^-}$ is the rate constant [mol L^{-1} s^{-1}], $K_{NO_3^-}$ and $K_{DOC,N}$ are Monod half saturation constants [mol L^{-1}], I_{O_2} is the inhibition constant for O_2 on denitrification [mol L^{-1}], f_{T,NO_3^-} is a factor including temperature effects on the reaction rate normalized to 20°C [-], T is temperature [°C], $\beta_{NO_3^-}$ is a calibration parameter influencing the rate of change for f_{T,NO_3^-} with temperature [°C^{-1}], T_{opt} is the temperature at which the reaction rate is the fastest [°C], and $c_{b,NO_3^-,j}$ is the normalized concentration of denitrifying bacteria in subsurface zone j [-]. The measurements showed that denitrification was mostly limited to the lower permeable aquifer zone around wells B3/2 and D3/2 (see Section 3.2). Therefore, $c_{bl,NO_3^-,BD}$ was set to 1 in the LK zone with x > -30 m (i.e., starting between well rows A and B). For the remaining subsurface zones $c_{b,NO_3^-,rest}$ < 1 was a calibration parameter.

For simplification, DOC concentrations were assumed to have limited influence on the reaction rates (K_{DOC,O_2} and $K_{DOC,N}$ set to 10^{-6} mol/L). Additionally, T_{opt} was set to 35°C as in previous studies (Knabe et al., 2021; Sharma et al., 2012).

2.6 Simulation of colloid-based Virus and Bacteria Transport

The reactive transport model for viruses (somatic coliphages and adenovirus) and bacteria (coliforms) accounts for kinetic sorption and desorption (attachment and detachment), inactivation, and straining. A one-site model was employed for coliforms, somatic coliphages and adenoviruses. Additionally, a two-site model was tested for coliforms, for which more data were available. Using the first-order rate equations typical for field-scale transport models for viruses and bacteria leads to (Hornstra et al., 2018; Torkzaban et al., 2019):

$$-\frac{dc_i}{dt} = r_{c_i} = k_{att,1,i} \cdot c_i - k_{det,1,i} \cdot S_{1,i} + k_{att,2,i} \cdot c_i - k_{det,2,i} \cdot S_{2,i} + \\ + k_{in.i,m} \cdot c_i + k_{str,i,j} \cdot c_i \quad (9)$$

$$-\frac{dS_{1,i}}{dt} = r_{S_i} = -k_{att,1,i} \cdot c_i + k_{det,1,i} \cdot S_{1,i} + z_{in,i.im}\, k_{in.i,m} \cdot S_{1,i} \quad (10)$$

$$-\frac{dS_{2,i}}{dt} = r_{S_i} = -k_{att,2,i} \cdot c_i + k_{det,2,i} \cdot S_{2,i} + z_{in,i.im}\, k_{in.i,m} \cdot S_{2,i} \quad (11)$$

where c_i is the concentration of species i in the water phase [viruses L^{-1}] or [bacteria L^{-1}], $S_{1/2,i}$ is the concentration of species i attached to the sediment at sites 1 or 2 respectively, expressed with respect to the solute volume [viruses L^{-1}] or [bacteria L^{-1}], $k_{att,1/2,i}$ and $k_{det,1/2,i}$ are the attachment and detachment coefficients of species i at sites 1 or 2 respectively [s^{-1}], $k_{in,i,m}$ is the inactivation coefficient of species i in the water phase (m) [s^{-1}], $z_{in,i,m}$ is the ratio of the inactivation coefficient in the immobile phase to the mobile phase for species i [-], and $k_{str,i,j}$ is the straining coefficient for species i in zone j [s^{-1}].

Adenovirus concentrations were measured via ddPCR (see Section 2.1) and therefore include active and inactive viruses. Thus, $k_{in.i,m}$ represents decay rather than inactivation for adenoviruses.

The attachment coefficient was calculated using Colloid-Filtration-Theory (Tufenkji and Elimelech, 2004):

$$k_{att,k,i} = \frac{3}{2} \cdot \frac{(1-\theta)}{d_{g,j}} \cdot \eta \cdot \alpha_{k,i} \cdot v \quad (12)$$

where θ is the volumetric water content [-], $d_{g,j}$ is the effective grain diameter in subsurface zone j [m], η is the collision efficiency [-], $\alpha_{k,i}$ is the attachment efficiency of species i at attachment site k [-], and v is the mean particle velocity [m s^{-1}]. η was calculated for every time step and cell using the equation proposed by Messina et al. (2015). $\alpha_{k,i}$ was a calibration parameter for each species. To use the mean particle velocity in PFLOTRAN's Reaction Sandbox calculations, a source code addition was necessary, which can be found at https://bitbucket.org/dknabe/pflotran-darcy-velocity-in-reaction-sandbox/branch/dustin/darcy-velocity-in-reaction-sandbox. For the two-site model applied solely to the coliforms, the first site was assumed to be a high turnover site (higher α and higher detachment coefficient), while the second site was assumed to be a low turnover site (lower α and lower detachment coefficient).

Straining was assumed to occur only at the colmation layer due to the lower grain size. Similarly, straining was assumed to be only significant for bacteria due to the smaller size of viruses. Straining was calculated following Bradford et al. (2003), but without the depth-dependency, as this does not fit to field-scale observations. However, the mean particle velocity was added because straining like attachment (eq. 12) depends on the amount of pore space passed and not on the travel time. This leads to:

$$k_{str,i,j} = p_{str} \cdot v \cdot \left(\frac{d_{p,i}}{d_{g,j}}\right)^{1.42} \quad (13)$$

where p_{str} is the straining constant [m^{-1}], v is the mean particle velocity [m s^{-1}], $d_{p,i}$ is the diameter of species i [m], and $d_{g,j}$ is the effective grain diameter in subsurface zone j [m].

The species-specific particle diameter and density were set based on the literature, with 1 µm and 1.12 g/cm³ for coliforms (Lewis et al., 2014; Ouzounov et al., 2016), 60 nm and 1.36 g/cm³ for somatic coliphages (Burbano-Rosero et al., 2011; Hafenstein and Fane, 2002), and 95 nm and 1.33 g/cm³ for adenovirus (Rafie et al., 2021; Sprinzl et al., 2001).

To reduce the number of calibration parameters, the effective grain diameter of each subsurface zone was defined based on their grain size classification. For the aquitard and the soil zone (both composed of silty fine sand), the effective diameter was set to 0.1 mm. For the sand-gravel aquifer, the effective diameter for the high permeable zone (coarse sand and gravel) was set to 1.12 mm (log-average size of coarse sand). For the low permeable zone (higher medium sand fraction), the effective diameter was set to 0.355 mm (log-average size of medium sand). For the colmation layer, the effective diameter was related to the permeability. Schubert (2002) reported that the clogged areas at the site are mainly silt. Therefore, the effective diameter for a stronger clogged colmation layer (assumed for permeability below 10^{-12} m^2) was set to 0.006 mm, and for a fully unclogged colmation layer similar to the aquifer (assumed for permeability of 10^{-10} m^2), the effective diameter was set to 1 mm, with a double log-linear interpolation for permeability values in between.

Studies have shown that under anoxic conditions, inactivation of viruses and bacteria can be lower (Frohnert et al., 2014; Gordon and Toze, 2003). This effect was considered for the model termed TV-O (applied only for coliforms). The inactivation coefficient in the mobile phase was calculated for the TV-O model with a step function:

$$k_{in,i,m}(c_{O_2}) = k_{in,i,m,0} \cdot \begin{cases} 1 & , c_{O_2} \geq c_{O_2,thr} \\ f_{anoxic} & , c_{O_2} < c_{O_2,thr} \end{cases} \quad (14)$$

where $k_{in,i,m,0}$ is the inactivation coefficient of species *i* in the mobile phase under oxic conditions [1 s^{-1}], c_{O_2} is the concentration of dissolved oxygen [molL^{-1}], $c_{O_2,thr}$ is the threshold concentration of dissolved oxygen for the inactivation coefficient [mol L^{-1}], and f_{anoxic} is the ratio of the inactivation coefficient between oxic and anoxic conditions [-].

Coliform bacteria include species, that can not only survive but also grow in the environment (Reitter et al., 2021). For the model termed TV-N, the hypothesis of coliform growth via denitrification (Bueno et al., 2018) was tested where eq. (10) was expanded to:

$$-\frac{dS_{1,i}}{dt} = r_{S_i} = -k_{att,1,i} \cdot c_i + k_{det,1,i} \cdot S_{1,i} + z_{in,i.im}\, k_{in.i,m} \cdot S_{1,i} - r_{NO_3^-} \cdot y \quad (15)$$

where $r_{NO_3^-}$ is the denitrification rate (eq. 7) [mol L^{-1} s^{-1}], and y is the coliform yield per mol NO_3^- reduced [bacteria mol^{-1}].

The grown coliforms were assumed to be at first immobile, because the bacteria facilitating the denitrification were also immobile. It was also assumed that coliform growth has no impact on the denitrification rate, because coliform concentrations are too low.

2.7 Model Calibration Strategy

Model parameters were calibrated using particle swarm optimization (PSO) (Robinson & Rahmat-Samii, 2004), a stochastic evolutionary algorithm that has been shown to yield robust results for environmental models with high numbers of parameters (Majone et al., 2012; Russian et al., 2019). The algorithm was employed as previously in Knabe et al. (2021), which followed Robinson & Rahmat-Samii (2004). A short description of the algorithm is provided in Supporting Information S1. For each PSO calibration, 24 particles and 30 displacements (iterations) were employed. Numerical tests showed that this was a good compromise between final objective function value (result quality) and computational time. Figure 2 shows the multi-stepped calibration strategy as well as calibrated and fixed parameters. The parameters of the solution with the lowest objective function were retained for the next calibration step. First, the hydraulic and conservative transport parameters were calibrated using the observations of piezometric pressure head, temperature, chloride, and electrical conductivity (EC). Afterwards, the reactive transport parameters for oxygen and nitrate consumption were calibrated, followed by the virus and bacteria transport parameters for each species independently. Three PSO calibrations were performed for each step and model, which allows to identify highly uncertain parameters.

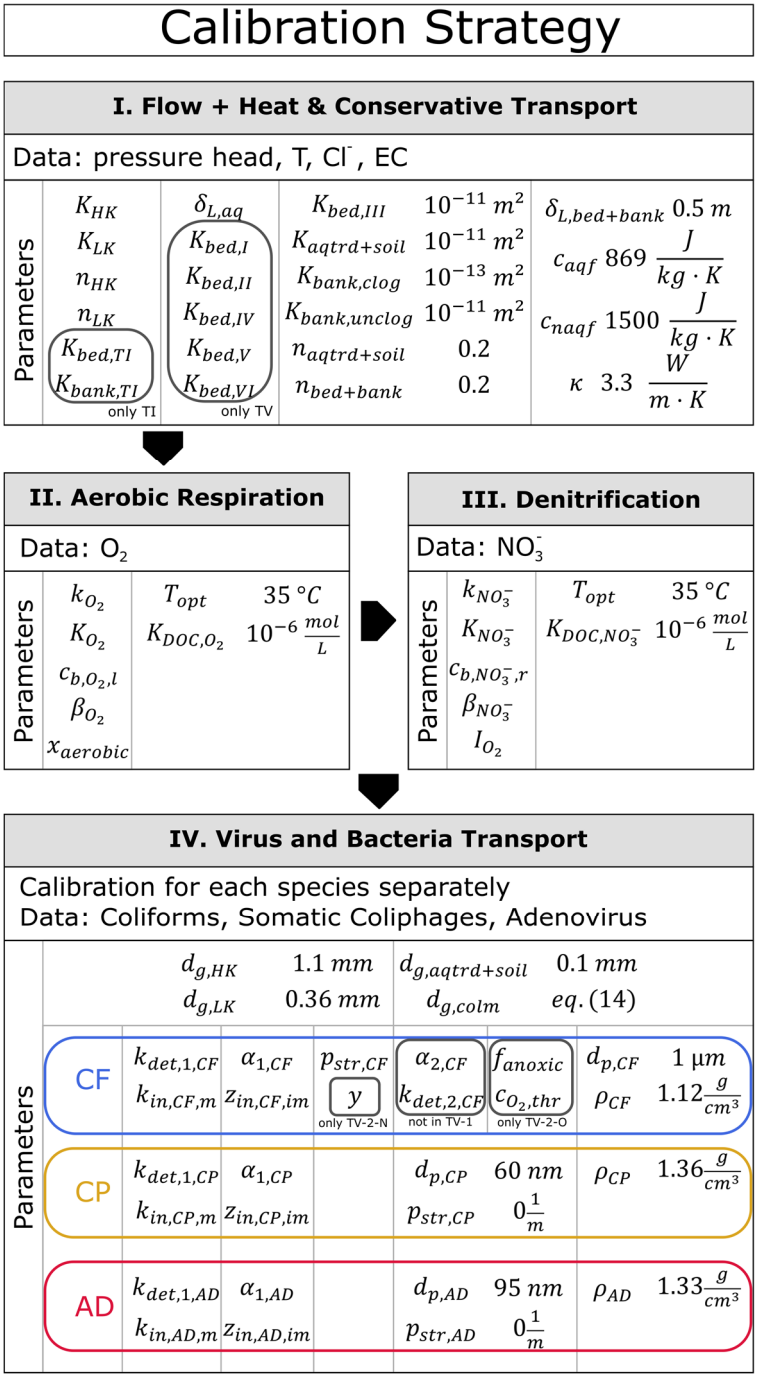

Figure 1. Calibration steps with associated data, calibrated and fixed parameters. Circled parameters are either species-specific (coliforms = CF, somatic coliphages = CP, adenovirus = AD) or only part of some models, e.g., TV or TI. For allowed range of calibrated parameters in the PSO see Supporting Information S2.

The objective function to be minimized in the calibration was defined with

$$\phi = \sum_k w_k \cdot \phi_k \tag{16}$$

where ϕ_k is the partial objective function from target output variable k (for example, temperature or concentration of coliforms), and w_k is the weight associated with target output variable k.

The partial objective function was defined with:

$$\phi_k = \frac{1}{N_k}\left(\sum_{\boldsymbol{x}}\left(\sum_t\left(\frac{f_{m,k}(\boldsymbol{x},t) - f_{o,k}(\boldsymbol{x},t)}{\max\limits_{\boldsymbol{x},t} f_{o,k} - \min\limits_{\boldsymbol{x},t} f_{o,k}}\right)^2\right)\right) \tag{17}$$

where $f_{m,k}(\boldsymbol{x},t)$ is the model output and $f_{o,k}(\boldsymbol{x},t)$ is the observed value of target output variable k at location x and time t, $\max\limits_{\boldsymbol{x},t} f_{o,k}$ and $\min\limits_{\boldsymbol{x},t} f_{o,k}$ are the maximum and minimum observed values of target variable k, and N_k is the total number of observations for target output variable k. ϕ_k can be interpreted as squared normalized residual averaged over all observation locations x and times t.

For microbiological measurements with no detection (i.e., concentration below detection limit (LOD)), $f_{o,k}(\boldsymbol{x},t)$ was set to the LOD and negative residuals (i.e., when $f_{m,k}(\boldsymbol{x},t) < LOD$) were set to zero. Thus, for a measured observation below LOD, all model output values below LOD are equally valid.

Weighting was only necessary in the multi-variable calibration at the beginning, using piezometric pressure head (w = 30), temperature (w = 10), chloride (w = 1), and EC (w = 1). Weights were set so that each variable provided a significant contribution to the objective function. Because of the normalization (eq. 17), higher weights indicate variables that fit observations better relative to their overall variability in the data.

3. Results and Discussion

3.1 Impact of hydrological events on hydraulics and conservative transport

3.1.1 Groundwater flow and heat transport

The simulation of water flow and heat transport was based on the measured data of hydraulic pressure heads and groundwater temperature (Figure 3a), both of which have a distinctive seasonality. The river level varied between 27.3 and 35.3 m.a.s.l. (meter above sea level), and the groundwater level varied, for example, between 26.8 and 33.7 m.a.s.l. at Observation Well C2. During winter and spring periods (periods I, II, V, VI), the river level was fluctuating substantially due to strong precipitation and snow melting events, the strongest leading to a river level increase of about 3 m in 7 days. In summer and fall 2018 (Period IV), the river level slowly decreased by about 2.5 m over 180 days because of increased air temperature and extended dry periods. The groundwater level followed the river level changes and fluctuations slightly dampened. For example, at Observation Well A3, the largest difference between groundwater level and river level was 1 m (during the heavy rain event in Period V), while in Period IV, the difference was only a few centimeters.

The heat transport from the river towards the production well is clearly visible. All riverside observation wells (rows A and B) show the river temperature trend only delayed and dampened (Figure 3a). River water temperature varied between 2.4 and 28.1°C, while at Observation Well A3, groundwater temperature varied between 5.3 and 25.3°C, with the summer temperature peak occurring 18 days later than in the river. In the landside observation wells (Row C), groundwater temperature remained mostly constant varying between 12.9 and 14.0°C, with two events where temperature dropped to about 8°C at Period I/II and Period VI. Those periods correlate with strong precipitation events and increasing river level. The observed temperature seasonality, including the high groundwater temperature differences between summer and winter (20°C), is comparable to published literature investigating similar environmental and geometric settings (Massmann et al., 2008a; Sheets et al., 2002). The differing trends in the landside and riverside observation wells indicate the different water sources: bank filtrate in the riverside and regional groundwater in the landside observation wells. The two low temperature events at Well Row C show that at strongly increasing river levels, bank filtrate can reach the landside observation wells. Water temperature at the production well was (as expected) a mixture between landside and riverside water temperatures. Both models, the TI and TV model, were able to simulate the measured piezometric pressure heads and temperature data very well. However, while the overall trend is captured, stronger temperature differences between model and measured data at the production well indicate that water mixing between bank filtrate and regional groundwater is not perfectly represented in the model.

For the observation wells containing both a PT- and a T-logger (0.5 m apart), the observed temperature differences between the loggers was mostly negligible (<0.4°C). However, in observation wells A1 and B1 during July/August 2018, the temperature difference reached up to 1.5°C. This difference likely results from the presence of colder water in the aquitard directly below A1 and B1.

During winter and spring periods, the river level pattern was the primary driver for groundwater flow velocity changes. The calculated Darcy velocities reached up to 6 m/day, with travel times as short as 7 days at B1 during a rapid river level incline (Figure 3a and b). The highest groundwater flow velocity and corresponding shortest travel time in winter 2017/18 (Period I) were not significantly different from those in winter 2018/19 (Period V/VI), despite the highest river level being 2 m higher in winter 2017/18. The pumping rate ranged between 400 and 1,000 m^3/day (for a single production well) and was the primary driver for groundwater flow velocity changes in summer and fall (Period IV). During Period IV, calculated Darcy velocities mostly remained around 2-3 m/day, and the travel time from the river to Observation Well B1 was never below 11 days. Between 10/04/2018 and 24/05/2018 (days 100-143, Period III), pumps were shut down for maintenance, and natural effluent conditions returned. Effluent conditions also occurred in short time period when the flood water receded in February 2018 (days 39-46). Compared to other results obtained for induced bank filtration sites, travel times at our site (mostly 7-20 days) range within medium to low values. Reported travel times at other induced bank filtration sites range from 2-3 days to several months (Kvitsand et al., 2017; Massmann et al., 2008b; Nagy-Kovács et al., 2019; Sheets et al., 2002).

3.1.2 Conservative transport

Both the TI and TV model showed a good match for the measurements of chloride and electrical conductivity (EC) (Figure 4). In general, chloride concentrations were similar in riverside (1.0-2.5 mmol/L) and landside observation wells (1.5-2.0 mmol/L, with some outliers at C1), although the trends showed differences. In contrast, stronger differences were observed for EC, ranging between 450-720 µS/cm for the riverside observation wells and 500-900 µS/cm (with a distinct maximum in

Period IV) for the landside observation wells. Model results and measured data show that chloride and EC of the river water are found in the riverside observation wells with a lag time of 1-2 weeks (e.g., mostly between 7-20 days for B1, Figure 4), which is in good agreement with the travel time calculations (Figure 3b). The mismatch between the conservative transport and measured data for EC at the production well (similarly observed for temperature) indicates that mixing between bank filtrate and regional groundwater is not perfectly captured in the model.

Model results and measured data for EC show the short effluent period during the waterworks maintenance. At days 134 and 148, the EC increased in Observation Well Row B. Such an increase cannot be observed in Well Row A and the river, indicating that during the waterworks maintenance, regional groundwater with higher EC has reached Well Row B, but not Well Row A.

3.1.3 Derived flow and conservative transport parameter

Model parameters were derived for the time-variant (TV) and time-invariant (TI) colmation layer models (Table 1). Results show that estimated permeabilities for both aquifer zones are similar in both models (TV: $8.3 \cdot 10^{-11}$ and $7.5 \cdot 10^{-10}$ m², TI: $1.3 \cdot 10^{-10}$ and $6.2 \cdot 10^{-10}$ m²) and with little uncertainty in the three PSO solutions. The obtained permeabilities are reasonable for alluvial gravel and sand mixtures (Miller et al., 2014). For the colmation layer in the TV model, the calibrated permeability obtained for Period I is relatively high ($1.2 \cdot 10^{-11}$, m²); for Period II, the calibrated permeability is very low ($1.1 \cdot 10^{-13}$ m²); for Period III, the permeability was fixed to simulate unclogged conditions ($5.0 \cdot 10^{-11}$ m²) due to the natural effluent conditions; and for Period IV, V, and VI, calibrated permeabilities range between $1.5 \cdot 10^{-12}$ and $3.9 \cdot 10^{-12}$ m². In contrast, the TI model results in a calibrated permeability for the riverbed of $1.7 \cdot 10^{-12}$ m² (roughly an average of the TV model calibrated permeabilities), and for the riverbank of $3.1 \cdot 10^{-13}$ m² (similar to the fixed value of 10^{-13} m² in the TV model). For Period I and part of Period VI, higher permeabilities derived with the TV model might have resulted from flooding events associated with higher flow velocity in the river (for Period VI, the flooding event immediately precedes it). These flooding events caused erosion/scouring of the colmation layer, a process that was also observed by Zhang et al. (2011). Ulrich et al. (2015) found that clogging mostly results from biological processes (biomass build-up). In our case, lower permeabilities occurred during warmer periods (IV), when biomass is more active. However, in periods II and V, estimated permeability was even lower. In general, the limited temporal resolution in our study of the colmation layer permeability (6 discrete time steps in 550 days) provides only an approximation of the dynamic changes to the colmation layer because controlling processes (physical clogging, bio-clogging, and erosion from the river) are varying at smaller time scales.

Calibrated porosities range between 0.2 (high permeability zone) and 0.3-0.4 (low permeability zone). Longitudinal dispersivity of the best fits for the TV and TI model differ — 2.8 m and 6.1 m, respectively. However, the uncertainty range for both is quite similar. Overall, the change in concentration of chloride and EC in the river over time was often small compared to the short travel times (often below 20 days for B, Figure 3b). An exception was the lower chloride concentration during Period V. The limited changes in chloride concentrations, linked with measurement errors and parameter correlations, led to the comparably higher uncertainty in conservative transport parameters.

525

526 *Table 1. Calibrated parameter values for the TV and TI models (best fit parameters in **bold**).*

Parameter	Unit	Model – PSO Solutions					
	ϕ/ϕ_{best}	TV			TI		
		3.6%	*3.9%*	*3.7%*	**0.0%**	*0.2%*	*1.3%*
K_{HK}	m^2	**7.5e-10**	*6.3e-10*	*7.5e-10*	**6.2e-10**	*6.8e-10*	*3.7e-10*
K_{LK}	m^2	**8.3e-11**	*9.9e-11*	*8.2e-11*	**1.3e-10**	*1.3e-10*	*1.9e-10*
$K_{bed,I}$	m^2	**1.2e-11**	*6.2e-11*	*1.5e-11*	**-**	-	-
$K_{bed,II}$	m^2	**1.1e-13**	*8.6e-13*	*1.3e-13*	**-**	-	-
$K_{bed,IV}$	m^2	**2.7e-12**	*3.2e-12*	*2.1e-12*	**-**	-	-
$K_{bed,V}$	m^2	**1.5e-12**	*2.1e-12*	*1.3e-12*	**-**	-	-
$K_{bed,VI}$	m^2	**3.9e-12**	*8.1e-12*	*2.9e-12*	**-**	-	-
$K_{bed,TI}$	m^2	**-**	-	-	**1.7e-12**	*2.1e-12*	*1.2e-11*
$K_{bank,TI}$	m^2	**-**	-	-	**3.1e-13**	*1.9e-13*	*9.4e-13*
n_{HK}	-	**0.25**	*0.22*	*0.17*	**0.25**	*0.21*	*0.35*
n_{LK}	-	**0.36**	*0.39*	*0.35*	**0.28**	*0.36*	*0.38*
$\delta_{L,aq}$	m	**2.8**	*3.7*	*6.6*	**6.1**	*2.8*	*7.5*

527

528

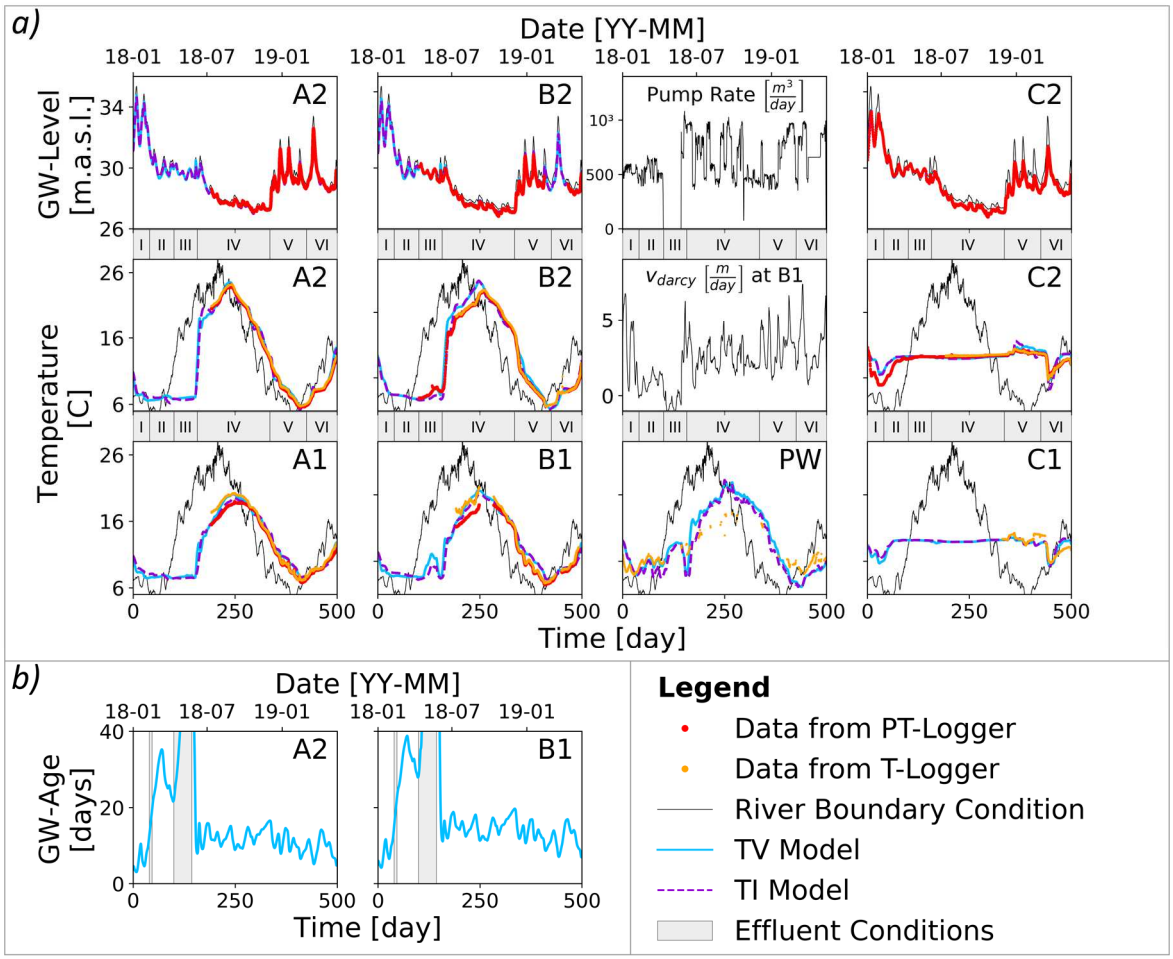

Figure 3. Data and model results for (a) pressure head and temperature, and (b) the groundwater age (mean travel time) at wells A2 and B1. Roman numerals indicate the time periods of the colmation layer for the TV model. For the full set of results for all observation wells see Supporting Information S3.

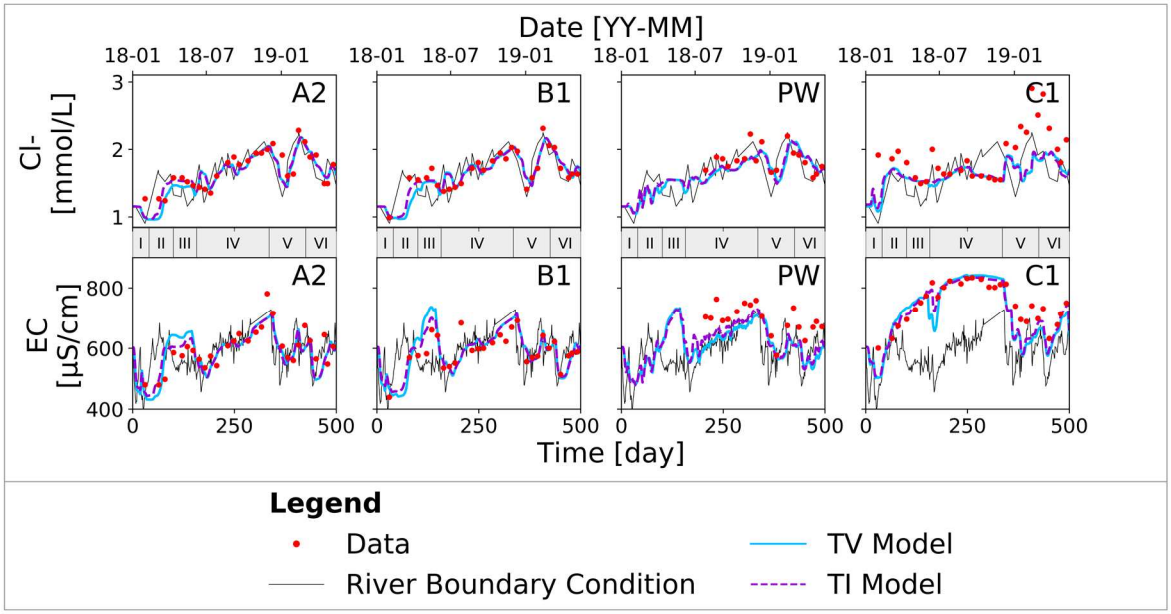

Figure 4. Data and model results for chloride and electrical conductivity (EC) at selected observation wells. Roman numerals indicate the time periods of the colmation layer for the TV model. For the full set of results for all observation wells see Supporting Information S3.

3.2 Reactive Transport of Dissolved Oxygen, Nitrate, and DOC

The reactive transport model fits the measured data for dissolved oxygen, nitrate, and DOC reasonably well. However, in summer, when oxygen consumption was highest, the model underestimates DOC concentrations. Aerobic respiration was assumed to be the primary process for DOC removal, but the DOC misfit indicates that the stoichiometric assumption with DOC as acetate is not fully correct and/or DOC was being affected by other processes.

Dissolved oxygen concentrations in river water and groundwater show a clear seasonal fluctuation, with lower concentrations prevailing in summer (Period IV) (Figure 5a) similar to the observations of Farnsworth and Hering (2011) and Massmann et al. (2008a). In groundwater, hypoxic conditions with oxygen concentrations near zero existed between July and September 2018. The mean difference between river water and groundwater was 0.15 mmol/L in winter and up to 0.25 mmol/L in summer. The larger difference between river water and groundwater in summer results from increased DOC degradation rates enabled by higher groundwater temperatures. The impact of temperature on the potential degradation rates is displayed by the 14-fold increase in f_{T,O_2} (eq. 4) between winter (5°C) and summer (25°C).

Oxygen concentrations decreased between river water and groundwater in the observation wells near the riverbank (Row A ≈ 40 m distance). However, further along the flow path, oxygen concentrations remain mostly constant (between observation wells A and B ≈ 20 m distance). The rapid oxygen decrease near the riverbank can be explained by higher microbiological activity closer to the river owing to increased nutrient concentrations or biofilm development within the colmation layer (Farnsworth and Hering, 2011; Mindl et al., 2015; Newcomer et al., 2016). The calibration of the reactive transport model estimated the extent of this high reactive zone (HRZ) as 6 - 8 m, and the reactivity ratio between the HRZ and the bulk aquifer as $c_{b,O2,low}$ < 0.02 (for all three PSO solutions). The results show that the HRZ is significantly larger than the colmation layer itself, and that downgradient of the HRZ, no significant reactions occurred.

*Table 1. Calibrated parameter values for aerobic respiration and denitrification in the TV model (best fit parameters in **bold**).*

		Model – PSO Solutions		
Parameter	ϕ/ϕ_{best} / **Unit**	**TV-O**		
		0.0%	*11.4%*	*3.4%*
k_{O_2}	$mol/(L \cdot day)$	**6.9e-10**	*2.3e-10*	*3.1e-10*
K_{O_2}	mol/L	**9.6e-04**	*7.5e-05*	*6.5e-04*
$c_{b,O_2,l}$	-	**2.7e-03**	*7.0e-03*	*1.4e-02*
β_{O_2}	$1/°C$	**0.23**	*0.16*	*0.21*
$x_{aerobic}$	m	**5.6**	*6.0*	*8.1*
Parameter	ϕ/ϕ_{best} / **Unit**	**TV-N**		
		0.0%	*0.0%*	*0.1%*
$k_{NO_3^-}$	$mol/(L \cdot day)$	**2.5e-11**	*2.4e-12*	*1.0e-11*
$K_{NO_3^-}$	mol/L	**1.9e-04**	*2.3e-05*	*1.7e-04*
$c_{b,NO_3^-,r}$	-	**8.1e-02**	*5.4e-02*	*2.6e-02*
$\beta_{NO_3^-}$	$1/°C$	**2.53**	*2.96*	*2.68*
I_{O_2}	mol/L	**1.5e-06**	*5.0e-06*	*3.9e-06*

In contrast to oxygen consumption, denitrification occurred only further along the flow path and was restricted to the late summer, when oxygen concentrations were very low. Denitrification was limited, observed only between days 230 and 250 in the lower permeable aquifer zone (observation wells B3, B2, D3 and D2; Figure 5b and Supporting Information S4). The spatial limitation of denitrification could be explained by a higher concentration of denitrifying bacteria in the zone around wells B3/2 and D3/2, which was potentially caused by the lower grain size and the slower flow velocity (possibly related to local heterogeneities as in Briggs et al. (2018)). The ratio between the denitrifying bacteria concentration in the bulk aquifer and the zone around B3/2 and D3/2 was calibrated with $c_{b,NO_3^-,rest}$ < 0.1 for all solutions. However, the estimated values for $\beta_{NO_3^-}$ between 2.5-3 would yield a rate increase by factor 100 for a temperature increase from 20 to 25°C. This

increase appears unrealistic and indicates that $\beta_{NO_3^-}$ was overfitted (stretched to unrealistic values), and that relevant processes such as growth or acclimation time of the denitrifying bacteria (Rivett et al., 2008) are missing in the model. However, since the nitrate concentration showed a good match with the experimental data, and since this paper focuses on virus and bacteria transport, this potential overfit for $\beta_{NO_3^-}$ was deemed acceptable.

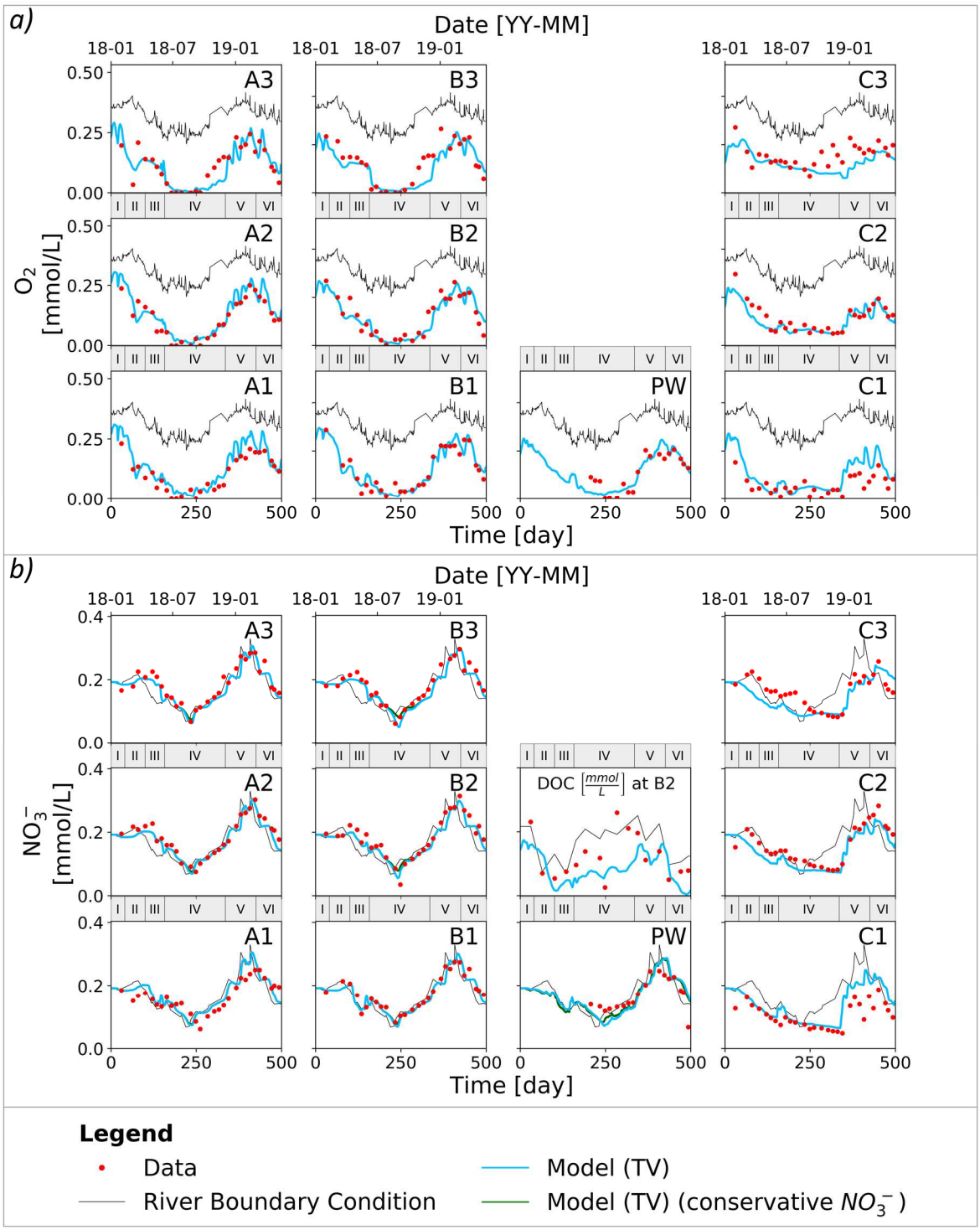

Figure 5. Data and model results for dissolved oxygen (a) and nitrate (b) at selected observation. b) also contains DOC at well B2 as single panel. Roman numerals indicate the time periods of the colmation layer for the TV model. For the full set of results for all observation wells see Supporting Information S4.

3.3 Reactive Transport of Adenovirus, Somatic Coliphages, and Coliforms

3.3.1 Detections in Surface and Groundwater

Multiple models were compared for the transport of coliforms (CF), somatic coliphages (CP), and adenovirus (AD) to determine key transport processes at field-scale in bank filtration. Figure 6 displays an overview of the calibrated model results and the experimental data.

Coliforms, somatic coliphages, and adenovirus were always found in the river, varying between 2 and 3 orders of magnitude over the monitoring period (CF: 99 – 24,132 MPN/100mL, CP: 0.8 – 115 PFU/100mL, AD: 70 – 114,805 copies/L). These concentrations are the result of the continuous influx of treated wastewater into the river. The AD concentrations are comparable to those reported by Betancourt et al. (2014). However, they are still below concentrations observed in rivers that are more intensely affected by urban activities. For example, Sprenger et al. (2014) measured about 300,000 copies/L AD and up to 189,000 PFU/100mL CP in a highly polluted river in Delhi (India). At our study site, no clear seasonal trends were observable for coliform and adenovirus concentrations in the river. However, somatic coliphage concentrations appeared to be lowest in late spring and early summer 2018 and highest in winter 2018/19.

In groundwater, coliforms were detected intermittently throughout the year, with higher concentrations in periods I and III (up to 419 MPN/100mL at Well Row A, detection limit = 1 MPN/100mL). Somatic coliphages were detected only at three times for both A2 and B1, all in winter (in periods I, V and VI with up to 1.5 PFU/100mL at A2, detection limit = 0.1 PFU/100mL). In contrast, adenovirus showed a relatively constant concentration at A2, ranging between 12 and 150 copies/L (some samples below detection limit), while not being detected at B1 (detection limit ≈ 10 copies/L).

These different detection patterns for coliforms, somatic coliphages, and adenovirus in groundwater indicate different transport behaviors during induced bank filtration. However, the measured detections for coliforms, somatic coliphages, and adenovirus are influenced by changes to their concentrations in the river. To account for the changing concentrations in the river and to focus on the transport processes, results are mainly shown as log-removals (Figure 6: log-difference between the concentration in observation well and the corresponding concentration in the river accounting for the conservative travel time). The full set of results in terms of concentrations are shown in Supporting Information S5.

3.3.2 Influence of Travel Time

As shown in Section 3.1, excluding times of effluent conditions, calculated travel times vary between 4 and 29 days in the riverside wells, with the shortest times in the winter periods I, V, and VI. It is known that shorter travel times favor lower removal, as inactivation occurs over time (e.g., De Roda Husman et al., 2009).

In fact, for somatic coliphages, the only three dates with detections in groundwater (at days 30, 344, and 492) are all associated with short travel times. The calculated removal from the better fitting CP-TV model follows the pattern of the travel times. According to the model, additional breakthroughs at low removal periods occurred during the winter 2018/19 (periods V and VI), basically during each heavy precipitation event. Further simulated breakthroughs with concentrations above the detection limit (days 363 and 385) were missed due to the sampling interval. However, at Day 407, the model estimates a breakthrough, and measurements exist at A2 and B1, but both were below detection limit (model overestimating by about 1 order of magnitude). This might result from a missing process in the model, or analytical errors in the measurements (at the well and/or the river boundary

condition). Nevertheless, the correlation is clear between detectable somatic coliphage concentrations in groundwater and periods with short travel times.

For coliforms, a better match for the CF-TV-2 model can be observed as it better replicates low removals (down to ca. 1 log-level for Row A, ca. 2 log-level for B1) and the measured breakthroughs at Day 30 (flood, winter 2017/18, Period I) and Day 163 (early summer 2018, Period III). Short travel times occurred at both Day 30 and Day 163. However, in winter 2018/19 (periods V and VI) removal remained high (at least between 3-4 log-levels) even when short travel times occurred as around Day 30 (Period I). Therefore, another process had become significant for coliform removal from winter 2017/18 to winter 2018/19.

In contrast to both coliforms and somatic coliphages, measured and simulated adenovirus were unaffected by travel time changes. In fact, model and experimental data show, over most of the simulated period, a relatively constant residual adenovirus concentration. The only minor exception to this is the initial flood (winter 2017/18, Period I). The influence of very short travel times in winter 2018/19 (periods V and VI) on the adenovirus concentration is indicated by the model results, but is much smaller compared to the measured and simulated somatic coliphage concentrations. This result indicates that safety distances for induced bank filtration sites (distance between river and well) calculated only from travel time and inactivation — as for example in Blaschke et al. (2016) — can lead to erroneous removal predictions for species whose removal is less influenced or not influenced by travel time, such as adenoviruses in our case.

3.3.3 Influence of a changing colmation layer

It was hypothesized that during the 16-month observation period, the colmation layer properties change, as a result of different hydrological or other environmental conditions (temperature, bio-clogging). The impact of the changing colmation layer can be analyzed by comparing the results of the TI and TV models. Overall, the TI model performed worse than the TV model, but this was stronger for coliforms (103% increased objective function compared to TV model) than for somatic coliphages (70%) and adenovirus (13%).

The removal of coliforms during periods V and VI (between 3-4 log-level at Well Row A and B) is high compared to the removal in Period I (about 1-2 log-level at Row A, 2-3 at Row B), where groundwater flow velocity, temperature, oxygen content, and even the coliforms concentration in the river were similar. The TI model fails to match this behavior, while the TV model fits the data well (Figure 6). Therefore, the stronger clogged colmation layer (resulting in increased attachment and straining) can explain the increased removal of coliforms between Period I and periods V/VI. For somatic coliphages and especially adenovirus, the effect of the colmation layer appears minor. Since coliforms are more than 10 times larger than somatic coliphages and adenovirus, it appears reasonable that they might be more affected by a lower effective grain size of the colmation layer (especially when considering straining as a removal process).

In Period III, natural effluent conditions occurred that were assumed to be leading to unclogging of the riverbank in the TV models. After the restart of the waterworks pumps, very high concentrations of coliforms were found in all riverside wells (Day 163), which afterwards quickly decreased for most wells below the detection limit (Day 177). Removal for coliforms during this period was limited to 0.5 log-level at A3 (even lower according to the model). Again, the CF-TV-2 model showed a good match with the data, while the CF-TI model failed. This shows that considering a changing colmation layer allowed for a better estimation of low removal for coliforms. As before, for somatic coliphages and adenovirus, no concentration increase was observed at or around Day 163. The CP-TV model reveals

682 that removal was low around Day 163. However, the somatic coliphage concentration in the river
683 was low during this time, resulting in concentrations below detection limit, and therefore a potential
684 increase at Day 163 could not be detected by the sampling.

685 To summarize, the colmation layer changes had a strong impact on coliform transport and a lower
686 impact on somatic coliphages, but no significant impact on adenovirus. Gupta et al. (2009) derived
687 from column experiments that scouring of the colmation layer during a flood event does not
688 significantly reduce bacteria removal, while Ramazanpour Esfahani et al. (2020) derived (also from
689 column experiments) that progressive clogging increased MS2 bacteriophage removal. Our results
690 agree with Ramazanpour Esfahani et al. (2020). However, direct observations of the time-dependent
691 changes in the permeability of the colmation layer are missing in our study. Future research at field-
692 scale should include direct observation to better identify the impact of the changing colmation layer
693 on pathogen transport.

694

695 #### 3.3.4 Influence of temperature, oxygen, and nitrate

696 The increased temperature in summer, in combination with increased biological activities, resulted in
697 low oxygen concentrations to fully anoxic conditions, potentially affecting virus and bacteria
698 transport. The reactive transport model was used to analyze the impact of these conditions on
699 coliform removal, but not on removal of somatic coliphages and adenovirus, because their
700 concentrations remained below detection limit during summer or remained relatively constant
701 throughout the observation period. Furthermore, for somatic coliphages and adenoviruses, the
702 calibrated models were able to match the data, without an additional effect based on temperature
703 or oxygen content.

704 During late summer and early autumn (days 230-270), there were several detections of coliforms
705 with little removal between A3/2 and B3/2 (5-10 MPN/100 mL, once at B3 43 MPN/100mL). When
706 concentrations increased in the river during late summer (reaching a high value of 15000-24000
707 MPN/100mL between days 220-250), the TV-2 and TI-2 models showed increased concentrations at
708 Well Row A, but not at Well Row B. The TV-2-O and TV-2-N models test the hypotheses that
709 inactivation might have been reduced under low oxygen concentrations (TV-2-O), and that
710 denitrification might have allowed growth of coliforms (TV-2-N). The results show that neither model
711 concepts, TV-2-O or TV-2-N, resulted in a significantly better match of the observed data than the
712 standard TV-2 model. The objective function for TV-2-O and TV-2-N only decreased by less than 2%.

713 Laboratory studies for bacteria and viruses have shown that higher temperatures typically lead to
714 higher inactivation (Anders and Chrysikopoulos, 2006; De Roda Husman et al., 2009), and that
715 absence of oxygen leads to lower inactivation (Frohnert et al., 2014). However, the impact of both
716 temperature and oxygen content on inactivation can be linked to the bioactivity (Gordon and Toze,
717 2003). In our study, coliforms had locally higher concentrations (lower removal) during the late
718 summer period (high temperatures, low oxygen content, occasional denitrification), but the standard
719 models (TV-2 and TI-2) underestimated the concentrations. This would indicate the effect of variable
720 oxygen concentration or denitrification. However, neither the TV-2-O nor the TV-2N model were able
721 to provide an improved fit. Given that coliform concentrations were high at both B3 and B2 around
722 Day 250, measurement or analytical errors are unlikely to be the cause. Therefore, the model is likely
723 missing an additional process, or the relationship between coliform inactivation and oxygen
724 concentration or denitrification is more complex than the implemented equations.

725

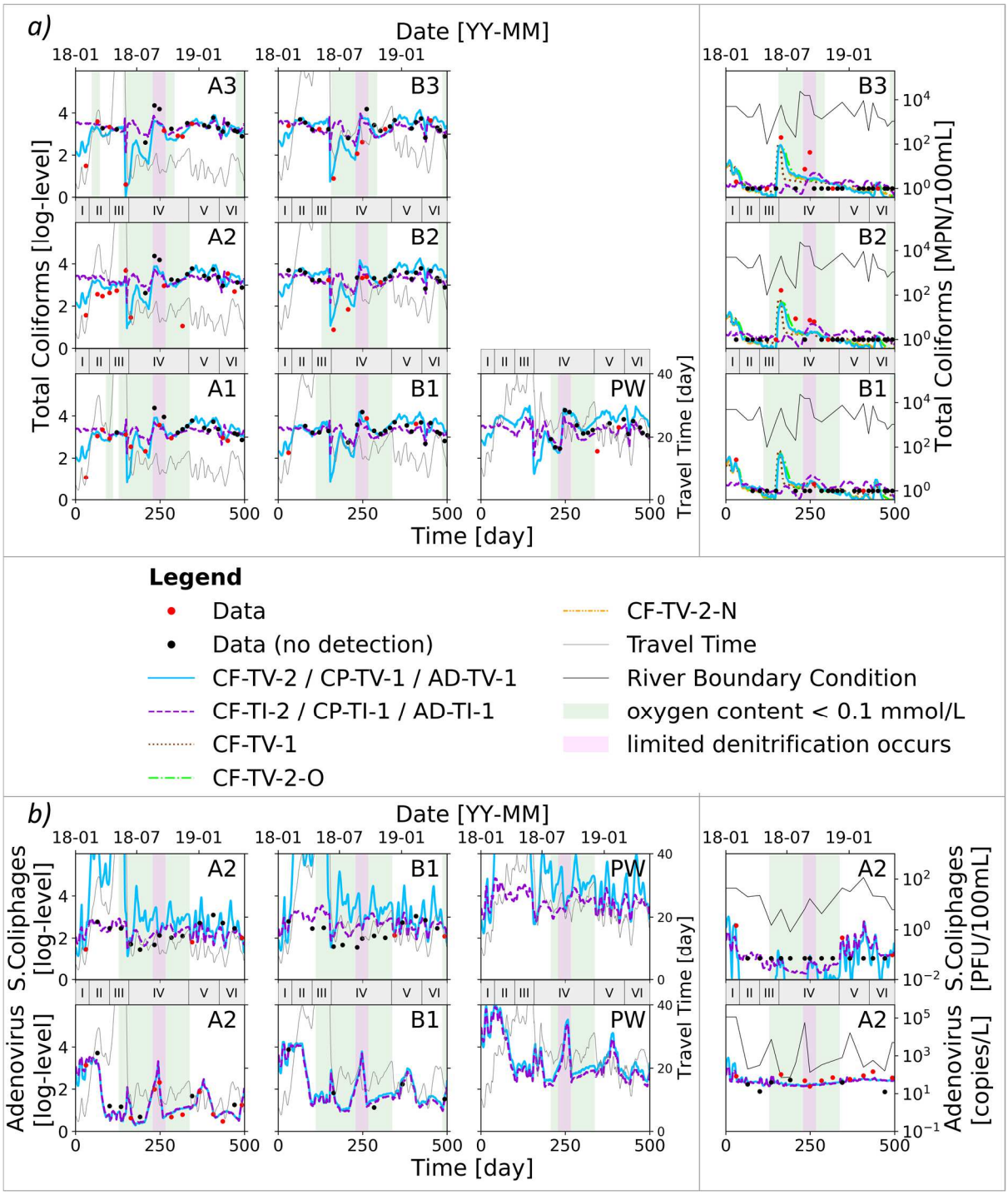

Figure 6. Data and modelling results for (a) coliforms (CF), (b) somatic coliphages (CP) and adenoviruses (AD) at selected observation wells. For the full set of results for all observation wells see Supporting Information S5.

3.3.5 Comparison between CF, CP, and AD

Previous studies — e.g., Knabe et al. (2021), Kvitsand et al. (2017), Weiss et al. (2005) — as well the results of this study show that the removal of viruses and bacteria during induced bank filtration can vary considerably over time and space. In our case, close to the riverbank (until Well A2), removal varied for coliforms between 1-4 log-levels, for somatic coliphages between 1-3, and for adenovirus between 0.5-3.5 (in log-level/m, CF: 0.025-0.1, CP: 0.025-0.075, AD: 0.013-0.087). In general, the removal rates (in terms of log-level/m) fit into those collected by Pang (2009) from the literature for aquifers of sand and gravel mixtures, and different viruses and bacteria, where most removal rates range between 0.005 to 0.1 log-level/m.

However, while the overall variation range for removal was similar for coliforms, somatic coliphages and adenovirus, the trends for removal over time were different. Somatic coliphage removal was shown to be primarily affected by travel time, which in turn was governed by the waterworks pumping rate and river level variations. For coliforms, the removal trend was similar in the beginning of the observation period (winter 2017/18 to summer 2018). Lower removal occurred at shorter travel times. However, especially in winter 2018/19, coliform removal was increased despite short travel times owing to an increased clogging of the colmation layer, leading to higher removal. In contrast, transport of adenovirus appeared always heavily buffered by the colmation layer, leading to a relatively constant adenovirus concentration close to the riverbank that decreased below the detection limit at some distance from the river. Thus, even high adenovirus concentrations in the river were not transported far into the riverbank. The calculated removal for adenovirus mainly reflects changes in the virus concentration in the river. Adenovirus removal was not affected by travel time, but increased with travel distance. Assuming adenovirus concentration in the groundwater close to the river (log-average ≈ 50 copies/L at A2, <10 copies/L at B1) is driven by the average concentration in the river (log-average ≈ 1000 copies/L), this leads to an average removal for adenovirus of 1.3 log-level (river to A2) and >1.7 (river to B1). This average removal of adenovirus is only about half the size of the transient removal of CF and CP (mostly between 2-4 log-level, but down to 0.5-1 at short travel times). However, since the transport behavior clearly differs among the pathogens, removal rates cannot be transferred from coliforms and somatic coliphages to adenoviruses.

The different transport behavior of coliforms, somatic coliphages, and adenovirus is the result of different key transport processes. The calibrated parameters (Table 3) show that transport of somatic coliphages, which was strongly affected by travel time, was dominated by inactivation (very high $k_{in,CP,m}$ with up to 1e-5 1/s). In contrast, coliforms were less affected by travel time and adenovirus were unaffected by travel time, and both show lower inactivation coefficients ($k_{in,AD,m}$ < 4e-7, and $k_{in,CF,m}$ around 2-4e-6 1/s for the better fitting TV-2 model). These inactivation coefficients are comparable to values found in the literature for similar species (De Roda Husman et al., 2009; Gordon and Toze, 2003; Hornstra et al., 2018; Schijven et al., 2013).

Attachment and detachment are similar for adenovirus and somatic coliphages, with slightly higher attachment for adenovirus (Table 3). The attachment efficiency α for adenovirus was around 8e-3 with k_{det} ca. 1e-8 1/s, while α for somatic coliphages was around 1-5e-3 and k_{det} around 1e-8 1/s, except for the best fit, where α was 0.05, but k_{det} was significantly higher with 4e-4 1/s. For coliforms, the one-site model CF-TV-1 resulted in similarly low α values around 1-2e-3 and k_{det} around 1-5e-8 1/s, while the two-site model CF-TV-2 resulted in an additional site with fast attachment and detachment (α at 0.1-0.7, and k_{det} at 0.7-7e-5 1/s). These values agree with those in Hornstra et al. (2018) and Kvitsand et al. (2015), where at some observation locations an additional fast attachment/detachment site was necessary to match the measured data.

Coliforms were considered to be additionally affected by straining in the colmation layer due to their larger size. The straining coefficients $p_{str,CF}$ for all coliform models were similar, mostly around 1e5 1/m, which appears relatively high, leading to first-order straining coefficients comparable to the higher values in Bradford and Bettahar (2005). In Oudega et al. (2021), bacteriophage *PhiX174* showed increased removal compared to bacterium *Bacillus subtilis*. In our data, removal of coliforms and somatic coliphages was quite similar in the first half of the observation period, but in the second half, removal of coliforms was higher than removal of somatic coliphages. During the second half of our observation period, removal of coliforms was increased, because the colmation layer was more clogged, increasing the effect of straining. This had no effect on the removal of somatic coliphages because of their smaller size. The increased removal of bacteriophages compared to bacteria in Oudega et al. (2021) is possibly related to weaker straining, since Oudega et al. (2021) conducted an injection experiment in a sand-gravel aquifer (i.e., without the presence of a colmation layer).

The difference between somatic coliphages and adenovirus transport was mainly a result of their different inactivation. However, adenovirus concentrations were measured via ddPCR and thus include active and inactive viruses. In contrast, measurements of coliforms and somatic coliphages identified only active bacteria/viruses. For adenoviruses, decay is observed rather than inactivation. Note that our model showed that inactivation was a primary removal mechanism for both coliforms and somatic coliphages. Boehm et al. (2019) compared the decay and inactivation rates of multiple viruses across the literature for surface waters. Their results show that for those virus groups, where data were available, inactivation rates (measured via cultivation) tended to be higher (up to an order of magnitude) than decay rates (measured via PCR). De Roda Husman et al. (2009) arrived at similar results studying poliovirus and coxsackievirus in artificial surface water and groundwater. This indicates that the different analysis techniques in our study for adenoviruses (via PCR) and for somatic coliphages (via cultivation) can be a factor in the observed differences in transport behavior. However, active adenovirus concentrations, relevant for infection risk, would be even lower than those measured by PCR, which were consistently always below the detection limit further into the riverbank (Well B1).

In summary, the transport of somatic coliphages was dominated by inactivation, the transport of adenovirus by attachment to and detachment from the sediment, and the transport of coliforms by straining and inactivation, as well as attachment to and detachment from the sediment.

*Table 3. Calibrated parameter values for the different virus and bacteria transport models (best fit parameters in **bold**, objective function values are relative to the best fit model for that species).*

		Model – PSO Solutions								
Parameter	ϕ/ϕ_{best} **Unit**	**CF-TV-2**			**CF-TI-2**			**CF-TV-1**		
		1.0%	*1.6%*	*6.5%*	**105.2%**	*105.7%*	*105.3%*	**11.6%**	*12.2%*	*12.8%*
$k_{in,CF,m}$	$1/s$	**4.2e-06**	*2.5e-06*	*2.7e-06*	**1.0e-07**	*1.1e-07*	*1.0e-07*	**1.3e-06**	*1.0e-06*	*4.2e-07*
$z_{in,CF,im}$	-	**1.9e-02**	*1.1e-02*	*3.0e-02*	**4.7e-01**	*5.2e-01*	*1.5e-02*	**1.4e-02**	*3.3e-02*	*9.1e-02*
$k_{det,1,CF}$	$1/s$	**3.8e-04**	*3.5e-04*	*7.6e-05*	**3.2e-05**	*5.8e-04*	*3.2e-04*	**4.1e-08**	*3.2e-08*	*1.8e-08*
$k_{det,2,CF}$	$1/s$	**5.1e-08**	*3.0e-08*	*7.7e-09*	**1.4e-07**	*7.7e-09*	*1.4e-07*	**-**	-	-
$\alpha_{1,CF}$	-	**6.8e-01**	*1.7e-01*	*1.1e-01*	**2.2e-02**	*1.3e-01*	*7.2e-02*	**9.8e-04**	*2.0e-03*	*1.8e-03*
$\alpha_{2,CF}$	-	**2.4e-03**	*2.0e-03*	*7.1e-03*	**3.1e-04**	*1.9e-03*	*2.0e-04*	**-**	-	-
$p_{str,CF}$	$1/m$	**7.7e+04**	*2.8e+05*	*1.8e+05*	**1.0e+05**	*8.9e+04*	*1.0e+05*	**3.0e+05**	*3.2e+05*	*3.9e+05*

Parameter	ϕ/ϕ_{best} **Unit**	**CF-TV-2-O**			**CF-TV-2-N**		
		2.6%	*10.0%*	*2.8%*	**0.0%**	*0.3%*	*1.0%*
$k_{in,CF,m}$	$1/s$	**2.6e-06**	*1.7e-06*	*3.4e-06*	**3.3e-06**	*3.8e-06*	*3.7e-06*
$z_{in,CF,im}$	-	**3.5e-02**	*1.8e-02*	*1.5e-02*	**1.5e-02**	*1.6e-02*	*2.7e-02*
$k_{det,1,CF}$	$1/s$	**1.5e-05**	*1.2e-05*	*9.0e-06*	**5.9e-05**	*7.2e-06*	*6.6e-05*
$k_{det,2,CF}$	$1/s$	**5.9e-09**	*6.4e-08*	*8.8e-09*	**4.5e-08**	*3.3e-08*	*6.4e-08*
$\alpha_{1,CF}$	-	**2.8e-02**	*1.5e-02*	*1.3e-02*	**9.2e-02**	*1.6e-02*	*1.1e-01*
$\alpha_{2,CF}$	-	**7.6e-03**	*3.6e-04*	*6.1e-03*	**1.8e-03**	*2.2e-03*	*1.9e-03*
$p_{str,CF}$	$1/m$	**1.6e+05**	*3.4e+05*	*1.5e+05*	**1.5e+05**	*9.7e+04*	*1.0e+05*
f_{anoxic}	-	**9.4e-01**	*7.7e-01*	*9.9e-01*	**-**	-	-
$c_{O_2,thr}$	mol/L	**6.2e+00**	*5.9e+00*	*1.4e+00*	**-**	-	-
y	bacteria/ mol	-	-	-	**2.7e4**	*1.9e5*	*2.0e5*

Parameter	ϕ/ϕ_{best} **Unit**	**CP-TV-1**			**CP-TI-1**		
		0.0%	*5.9%*	*5.7%*	**70.0%**	*71.3%*	*71.5%*
$k_{in,CP,m}$	$1/s$	**1.0e-05**	*5.9e-06*	*5.7e-06*	**2.8e-07**	*2.7e-06*	*2.7e-06*
$z_{in,CP,im}$	-	**6.9e-01**	*2.6e+00*	*4.2e+00*	**2.4e-01**	*2.8e-02*	*3.6e-02*
$k_{det,1,CP}$	$1/s$	**3.9e-04**	*4.9e-09*	*1.8e-07*	**9.2e-09**	*1.4e-08*	*1.8e-08*
$\alpha_{1,CP}$	-	**4.9e-02**	*1.6e-03*	*1.6e-03*	**2.5e-03**	*2.0e-03*	*2.0e-03*
Parameter	ϕ/ϕ_{best} **Unit**	**AD-TV-1**			**AD-TI-1**		
		0.0%	*1.0%*	*0.5%*	**13.0%**	*14.4%*	*15.8%*
$k_{in,AD,m}$	$1/s$	**6.3e-08**	*1.9e-08*	*2.2e-08*	**3.9e-07**	*1.7e-07*	*4.1e-08*
$z_{in,AD,im}$	-	**1.1e-02**	*7.2e-02*	*4.9e-02*	**1.1e-02**	*2.9e-02*	*1.4e-02*
$k_{det,1,AD}$	$1/s$	**8.2e-09**	*1.0e-08*	*9.0e-09*	**1.8e-08**	*1.7e-08*	*1.3e-08*
$\alpha_{1,AD}$	-	**8.3e-03**	*8.8e-03*	*8.5e-03*	**6.8e-03**	*6.8e-03*	*6.6e-03*

4. Conclusion

The numerical code PFLOTRAN was used to analyze data from a 16-month monitoring to identify key transport processes and seasonal patterns of adenovirus, somatic coliphages, and coliforms at induced riverbank filtration sites. Our main findings are:

- Travel time changes resulted during rainy seasons from rapidly rising river levels after strong precipitation or snow melt events, and during the dry season from changes in pumping rates.

- Shorter travel times reduced the removal efficiency for somatic coliphages and coliforms. However, adenovirus removal was independent of travel time but dependent on travel distance.
- Numerical analysis indicates that changes in the colmation/clogging layer permeability are coupled to the river stage but are also affected by waterworks maintenance periods (no pumping). Removal of coliforms was lower at higher colmation layer permeabilities (after a flood and after a maintenance period). However, removal of viruses (somatic coliphages and adenovirus) was independent of the colmation layer permeability.
- High groundwater temperatures and low oxygen concentrations associated with denitrification in late summer had no visible impact on removal of somatic coliphages and adenovirus. For coliforms, these conditions correlated with lower removal efficiencies. However, the numerical results did not support a correlation between lower oxygen concentrations and/or denitrification with lower coliform removal.

The limited number of detections of somatic coliphages in groundwater made it difficult to identify key removal processes and parameters. Additionally, uncertainty remains with respect to the concentration of active adenoviruses, which are relevant in estimating the risk for drinking water production, since our data contains information about total (active and inactive, i.e., infectious and non-infectious) adenovirus particles exclusively. But even the total adenovirus concentration remained below the detection limit at 40 m distance from the riverbank, and therefore the removal of active adenoviruses appears sufficient. Nevertheless, developing methods to analyze (active) human pathogenic viruses at low concentrations would greatly improve the data basis for modelling and risk analysis studies. Given that drinking water target concentrations for active viruses can be as low as 10^{-5} viruses per liter (WHO, 2017), methods to detect low concentrations of pathogenic viruses could be a key target for future research.

Acknowledgments

We would like to thank the Deutsche Bundesstiftung Umwelt (DBU) for financially supporting this study. We greatly appreciate the support of the Stadtwerke Düsseldorf for sample collection and non-virus-related sample analysis. The logged river data was thankfully provided by the German Bundesanstalt für Gewässerkunde. Additionally, we would like to thank the North-German Supercomputing Alliance (HLRN) for granting high performance computing resources. Dustin Knabe acknowledges the Geo.X network and the Watershed Function Science Focus Area project (funded by the U.S. Department of Energy, Office of Science, and Biological and Environmental Research under Contract No. DE-AC02-05CH11231) for supporting this study by providing funds for a research visit at Lawrence Berkeley National Laboratory. We thank Daniel Hawkes from Lawrence Berkeley National Laboratory for technical editing.

References

Anders, R., Chrysikopoulos, C. V., 2006. Evaluation of the factors controlling the time-dependent inactivation rate coefficients of bacteriophage MS2 and PRD1. Environ. Sci. Technol. 40, 3237–3242. https://doi.org/10.1021/es051604b

Arora, B., Spycher, N.F., Steefel, C.I., Molins, S., Bill, M., Conrad, M.E., Dong, W., Faybishenko, B., Tokunaga, T.K., Wan, J., Williams, K.H., Yabusaki, S.B., 2016. Influence of hydrological, biogeochemical and temperature transients on subsurface carbon fluxes in a flood plain environment. Biogeochemistry 127, 367–396. https://doi.org/10.1007/s10533-016-0186-8

Avasarala, S., Lichtner, P.C., Ali, A.M.S., González-Pinzón, R., Blake, J.M., Cerrato, J.M., 2017. Reactive Transport of U and v from Abandoned Uranium Mine Wastes. Environ. Sci. Technol. 51, 12385–12393. https://doi.org/10.1021/acs.est.7b03823

Betancourt, W.Q., Kitajima, M., Wing, A.D., Regnery, J., Drewes, J.E., Pepper, I.L., Gerba, C.P., 2014. Assessment of virus removal by managed aquifer recharge at three full-scale operations. J. Environ. Sci. Heal. - Part A Toxic/Hazardous Subst. Environ. Eng. 49, 1685–1692. https://doi.org/10.1080/10934529.2014.951233

Binder, T., 2013. Entwicklung einer Methode zur Anreicherung somatischer Coliphagen. DVGW Energ. | wasser-praxis 10, 26–30.

Blaschke, A.P., Derx, J., Zessner, M., Kirnbauer, R., Kavka, G., Strelec, H., Farnleitner, A.H., Pang, L., 2016. Setback distances between small biological wastewater treatment systems and drinking water wells against virus contamination in alluvial aquifers. Sci. Total Environ. 573, 278–289. https://doi.org/10.1016/j.scitotenv.2016.08.075

Boehm, A.B., Silverman, A.I., Schriewer, A., Goodwin, K., 2019. Systematic review and meta-analysis of decay rates of waterborne mammalian viruses and coliphages in surface waters. Water Res. 164, 114898. https://doi.org/https://doi.org/10.1016/j.watres.2019.114898

Bradford, S.A., Bettahar, M., 2005. Straining, Attachment, and Detachment of Cryptosporidium Oocysts in Saturated Porous Media . J. Environ. Qual. 34, 469–478. https://doi.org/10.2134/jeq2005.0469

Bradford, S.A., Harvey, R.W., 2017. Future research needs involving pathogens in groundwater. Hydrogeol. J. 25, 931–938. https://doi.org/10.1007/s10040-016-1501-0

Bradford, S.A., Simunek, J., Bettahar, M., Van Genuchten, M.T., Yates, S.R., 2003. Modeling colloid attachment, straining, and exclusion in saturated porous media. Environ. Sci. Technol. 37, 2242–2250. https://doi.org/10.1021/es025899u

Briggs, M.A., Day-Lewis, F.D., Dehkordy, F.M.P., Hampton, T., Zarnetske, J.P., Scruggs, C.R., Singha, K., Harvey, J.W., Lane, J.W., 2018. Direct Observations of Hydrologic Exchange Occurring With Less-Mobile Porosity and the Development of Anoxic Microzones in Sandy Lakebed Sediments. Water Resour. Res. 54, 4714–4729. https://doi.org/10.1029/2018WR022823

Bueno, E., Sit, B., Waldor, M.K., Cava, F., 2018. Anaerobic nitrate reduction divergently governs population expansion of the enteropathogen Vibrio cholerae. Nat. Microbiol. 3, 1346–1353. https://doi.org/10.1038/s41564-018-0253-0

Burbano-Rosero, E.M., Ueda-Ito, M., Kisielius, J.J., Nagasse-Sugahara, T.K., Almeida, B.C., Souza, C.P., Markman, C., Martins, G.G., Albertini, L., Rivera, I.N.G., 2011. Diversity of Somatic coliphages in coastal regions with different levels of anthropogenic activity in São Paulo state, Brazil. Appl. Environ. Microbiol. 77, 4208–4216. https://doi.org/10.1128/AEM.02780-10

De Roda Husman, A.M., Lodder, W.J., Rutjes, S.A., Schijven, J.F., Teunis, P.F.M., 2009. Long-term

900 inactivation study of three enteroviruses in artificial surface and groundwaters, using PCR and
901 cell culture. Appl. Environ. Microbiol. 75, 1050–1057. https://doi.org/10.1128/AEM.01750-08

902 Dillon, P., Stuyfzand, P., Grischek, T., Lluria, M., Pyne, R.D.G., Jain, R.C., Bear, J., Schwarz, J., Wang,
903 W., Fernandez, E., Stefan, C., Pettenati, M., van der Gun, J., Sprenger, C., Massmann, G.,
904 Scanlon, B.R., Xanke, J., Jokela, P., Zheng, Y., Rossetto, R., Shamrukh, M., Pavelic, P., Murray, E.,
905 Ross, A., Bonilla Valverde, J.P., Palma Nava, A., Ansems, N., Posavec, K., Ha, K., Martin, R.,
906 Sapiano, M., 2019. Sixty years of global progress in managed aquifer recharge. Hydrogeol. J. 27,
907 1–30. https://doi.org/10.1007/s10040-018-1841-z

908 Doppler, T., Franssen, H.-J.H., Kaiser, H.-P., Kuhlman, U., Stauffer, F., 2007. Field evidence of a
909 dynamic leakage coefficient for modelling river–aquifer interactions. J. Hydrol. 347, 177–187.
910 https://doi.org/https://doi.org/10.1016/j.jhydrol.2007.09.017

911 Dwivedi, D., Arora, B., Steefel, C.I., Dafflon, B., Versteeg, R., 2018a. Hot Spots and Hot Moments of
912 Nitrogen in a Riparian Corridor. Water Resour. Res. 54, 205–222.
913 https://doi.org/10.1002/2017WR022346

914 Dwivedi, D., Steefel, C.I., Arora, B., Newcomer, M., Moulton, J.D., Dafflon, B., Faybishenko, B., Fox, P.,
915 Nico, P., Spycher, N., Carroll, R., Williams, K.H., 2018b. Geochemical Exports to River From the
916 Intrameander Hyporheic Zone Under Transient Hydrologic Conditions: East River Mountainous
917 Watershed, Colorado. Water Resour. Res. 54, 8456–8477.
918 https://doi.org/10.1029/2018WR023377

919 Engeler, I., Hendricks Franssen, H.J., Müller, R., Stauffer, F., 2011. The importance of coupled
920 modelling of variably saturated groundwater flow-heat transport for assessing river–aquifer
921 interactions. J. Hydrol. 397, 295–305.
922 https://doi.org/https://doi.org/10.1016/j.jhydrol.2010.12.007

923 Engelhardt, I., Prommer, H., Schulz, M., Vanderborght, J., Schüth, C., Ternes, T.A., 2014. Reactive
924 transport of iomeprol during stream-groundwater interactions. Environ. Sci. Technol. 48, 199–
925 207. https://doi.org/10.1021/es403194r

926 European Union, 2020. DIRECTIVE (EU) 2020/2184 OF THE EUROPEAN PARLIAMENT AND OF THE
927 COUNCIL of 16 December 2020 on the quality of water intended for human consumption
928 (recast) (Text with EEA relevance), Official Journal of the European Union.

929 Farnsworth, C.E., Hering, J.G., 2011. Inorganic Geochemistry and Redox Dynamics in Bank Filtration
930 Settings. Environ. Sci. Technol. 45, 5079–5087. https://doi.org/10.1021/es2001612

931 Frohnert, A., Apelt, S., Klitzke, S., Chorus, I., Szewzyk, R., Selinka, H.-C., 2014. Transport and removal
932 of viruses in saturated sand columns under oxic and anoxic conditions – Potential implications
933 for groundwater protection. Int. J. Hyg. Environ. Health 217, 861–870.
934 https://doi.org/https://doi.org/10.1016/j.ijheh.2014.06.004

935 Gardner, W.P., Hammond, G., Lichtner, P., 2015. High Performance Simulation of Environmental
936 Tracers in Heterogeneous Domains. Groundwater 53, 71–80.
937 https://doi.org/10.1111/gwat.12148

938 Gillefalk, M., Massmann, G., Nützmann, G., Hilt, S., 2018. Potential Impacts of Induced Bank Filtration
939 on Surface Water Quality: A Conceptual Framework for Future Research. Water 10, 1240.
940 https://doi.org/10.3390/w10091240

941 Goode, D.J., 1996. Direct simulation of groundwater age. Water Resour. Res. 32, 289–296.
942 https://doi.org/10.1029/95WR03401

943 Gordon, C., Toze, S., 2003. Influence of groundwater characteristics on the survival of enteric viruses.
944 J. Appl. Microbiol. 95, 536–544. https://doi.org/https://doi.org/10.1046/j.1365-

945 2672.2003.02010.x

946 Gupta, V., Johnson, W.P., Shafieian, P., Ryu, H., Alum, A., Abbaszadegan, M., Hubbs, S.A., Rauch-
947 Williams, T., 2009. Riverbank filtration: Comparison of pilot scale transport with theory.
948 Environ. Sci. Technol. 43, 669–676. https://doi.org/10.1021/es8016396

949 Hafenstein, S., Fane, B.A., 2002. ϕX174 Genome-Capsid Interactions Influence the Biophysical
950 Properties of the Virion: Evidence for a Scaffolding-Like Function for the Genome during the
951 Final Stages of Morphogenesis. J. Virol. 76, 5350–5356. https://doi.org/10.1128/jvi.76.11.5350-
952 5356.2002

953 Hammond, G.E., Lichtner, P.C., Mills, R.T., 2014. Evaluating the performance of parallel subsurface
954 simulators: An illustrative example with PFLOTRAN. Water Resour. Res. 50, 208–228.
955 https://doi.org/https://doi.org/10.1002/2012WR013483

956 Hammond, G.E., Lichtner, P.C., Rockhold, M.L., 2011. Stochastic simulation of uranium migration at
957 the Hanford 300 Area. J. Contam. Hydrol. 120–121, 115–128.
958 https://doi.org/10.1016/j.jconhyd.2010.04.005

959 Hester, E.T., Young, K.I., Widdowson, M.A., 2013. Mixing of surface and groundwater induced by
960 riverbed dunes: Implications for hyporheic zone definitions and pollutant reactions. Water
961 Resour. Res. 49, 5221–5237. https://doi.org/https://doi.org/10.1002/wrcr.20399

962 Hornstra, L.M., Schijven, J.F., Waade, A., Prat, G.S., Smits, F.J.C., Cirkel, G., Stuyfzand, P.J., Medema,
963 G.J., 2018. Transport of bacteriophage MS2 and PRD1 in saturated dune sand under suboxic
964 conditions. Water Res. 139, 158–167.
965 https://doi.org/https://doi.org/10.1016/j.watres.2018.03.054

966 Hu, B., Teng, Y., Zhai, Y., Zuo, R., Li, J., Chen, H., 2016. Riverbank filtration in China: A review and
967 perspective. J. Hydrol. 541, 914–927.
968 https://doi.org/https://doi.org/10.1016/j.jhydrol.2016.08.004

969 Huggett, J.F., 2020. The Digital MIQE Guidelines Update: Minimum Information for Publication of
970 Quantitative Digital PCR Experiments for 2020. Clin. Chem. 66, 1012–1029.
971 https://doi.org/10.1093/clinchem/hvaa125

972 Hunt, R.J., Johnson, W.P., 2017. Pathogen transport in groundwater systems: contrasts with
973 traditional solute transport. Hydrogeol. J. 25, 921–930. https://doi.org/10.1007/s10040-016-
974 1502-z

975 ISO 9308-2, 1990. Water quality – Detection and enumeration of coliform organisms, thermotolerant
976 coliform organisms and presumptive Escherichia coli – Part 2: Multiple tube (most probable
977 number) method, 9308-2:1990.

978 Johnson, W.P., Rasmuson, A., Pazmiño, E., Hilpert, M., 2018. Why Variant Colloid Transport Behaviors
979 Emerge among Identical Individuals in Porous Media When Colloid-Surface Repulsion Exists.
980 Environ. Sci. Technol. 52, 7230–7239. https://doi.org/10.1021/acs.est.8b00811

981 Knabe, D., Guadagnini, A., Riva, M., Engelhardt, I., 2021. Uncertainty Analysis and Identification of
982 Key Parameters Controlling Bacteria Transport Within a Riverbank Filtration Scenario. Water
983 Resour. Res. 57, e2020WR027911. https://doi.org/https://doi.org/10.1029/2020WR027911

984 Kvitsand, H.M.L., Ilyas, A., Østerhus, S.W., 2015. Rapid bacteriophage MS2 transport in an oxic sandy
985 aquifer in cold climate: Field experiments and modeling. Water Resour. Res. 51, 9725–9745.
986 https://doi.org/https://doi.org/10.1002/2015WR017863

987 Kvitsand, H.M.L., Myrmel, M., Fiksdal, L., Østerhus, S.W., 2017. Evaluation of bank filtration as a
988 pretreatment method for the provision of hygienically safe drinking water in Norway: results

989 from monitoring at two full-scale sites. Hydrogeol. J. 25, 1257–1269.
990 https://doi.org/10.1007/s10040-017-1576-2

991 Lewis, C.L., Craig, C.C., Senecal, A.G., 2014. Mass and density measurements of live and dead gram-
992 negative and gram-positive bacterial populations. Appl. Environ. Microbiol. 80, 3622–3631.
993 https://doi.org/10.1128/AEM.00117-14

994 Maeng, S.K., Sharma, S.K., Lekkerkerker-Teunissen, K., Amy, G.L., 2011. Occurrence and fate of bulk
995 organic matter and pharmaceutically active compounds in managed aquifer recharge: A review.
996 Water Res. 45, 3015–3033. https://doi.org/https://doi.org/10.1016/j.watres.2011.02.017

997 Majone, B., Bovolo, C.I., Bellin, A., Blenkinsop, S., Fowler, H.J., 2012. Modeling the impacts of future
998 climate change on water resources for the Gállego river basin (Spain). Water Resour. Res. 48.
999 https://doi.org/https://doi.org/10.1029/2011WR010985

1000 Massmann, G., Nogeitzig, A., Taute, T., Pekdeger, A., 2008a. Seasonal and spatial distribution of
1001 redox zones during lake bank filtration in Berlin, Germany. Environ. Geol. 54, 53–65.
1002 https://doi.org/10.1007/s00254-007-0792-9

1003 Massmann, G., Sültenfuß, J., Dünnbier, U., Knappe, A., Taute, T., Pekdeger, A., 2008b. Investigation of
1004 groundwater residence times during bank filtration in Berlin: A multi-tracer approach. Hydrol.
1005 Process. 22, 788–801. https://doi.org/10.1002/hyp.6649

1006 Messina, F., Marchisio, D.L., Sethi, R., 2015. An extended and total flux normalized correlation
1007 equation for predicting single-collector efficiency. J. Colloid Interface Sci. 446, 185–193.
1008 https://doi.org/10.1016/j.jcis.2015.01.024

1009 Miller, R.B., Heeren, D.M., Fox, G.A., Halihan, T., Storm, D.E., Mittelstet, A.R., 2014. The hydraulic
1010 conductivity structure of gravel-dominated vadose zones within alluvial floodplains. J. Hydrol.
1011 513, 229–240. https://doi.org/10.1016/j.jhydrol.2014.03.046

1012 Mindl, B., Hofer, J., Kellermann, C., Stichler, W., Teichmann, G., Psenner, R., Danielopol, D.L.,
1013 Neudorfer, W., Griebler, C., 2015. Evaluating the performance of water purification in a
1014 vegetated groundwater recharge basin maintained by short-Term pulsed infiltration events.
1015 Water Sci. Technol. 72, 1912–1922. https://doi.org/10.2166/wst.2015.400

1016 Montazeri, N., Goettert, D., Achberger, E.C., Johnson, C.N., Prinyawiwatkul, W., Janes, M.E., 2015.
1017 Pathogenic enteric viruses and microbial indicators during secondary treatment of municipal
1018 wastewater. Appl. Environ. Microbiol. 81, 6436–6445. https://doi.org/10.1128/AEM.01218-15

1019 Morrison, C.M., Betancourt, W.Q., Quintanar, D.R., Lopez, G.U., Pepper, I.L., Gerba, C.P., 2020.
1020 Potential indicators of virus transport and removal during soil aquifer treatment of treated
1021 wastewater effluent. Water Res. 177, 115812.
1022 https://doi.org/https://doi.org/10.1016/j.watres.2020.115812

1023 Nagy-Kovács, Z., Davidesz, J., Czihat-Mártonné, K., Till, G., Fleit, E., Grischek, T., 2019. Water Quality
1024 Changes during Riverbank Filtration in Budapest, Hungary. Water 11, 302.
1025 https://doi.org/10.3390/w11020302

1026 Navarre-Sitchler, A.K., Maxwell, R.M., Siirila, E.R., Hammond, G.E., Lichtner, P.C., 2013. Elucidating
1027 geochemical response of shallow heterogeneous aquifers to CO2 leakage using high-
1028 performance computing: Implications for monitoring of CO2 sequestration. Adv. Water Resour.
1029 53, 45–55. https://doi.org/10.1016/j.advwatres.2012.10.005

1030 Newcomer, M.E., Hubbard, S.S., Fleckenstein, J.H., Maier, U., Schmidt, C., Thullner, M., Ulrich, C.,
1031 Flipo, N., Rubin, Y., 2016. Simulating bioclogging effects on dynamic riverbed permeability and
1032 infiltration. Water Resour. Res. 52, 2883–2900.
1033 https://doi.org/https://doi.org/10.1002/2015WR018351

Oudega, T.J., Lindner, G., Derx, J., Farnleitner, A.H., Sommer, R., Blaschke, A.P., Stevenson, M.E., 2021. Upscaling Transport of Bacillus subtilis Endospores and Coliphage phiX174 in Heterogeneous Porous Media from the Column to the Field Scale. Environ. Sci. Technol. 55, 11060–11069. https://doi.org/10.1021/acs.est.1c01892

Ouzounov, N., Nguyen, J.P., Bratton, B.P., Jacobowitz, D., Gitai, Z., Shaevitz, J.W., 2016. MreB Orientation Correlates with Cell Diameter in Escherichia coli. Biophys. J. 111, 1035–1043. https://doi.org/https://doi.org/10.1016/j.bpj.2016.07.017

Pang, L., 2009. Microbial Removal Rates in Subsurface Media Estimated From Published Studies of Field Experiments and Large Intact Soil Cores. J. Environ. Qual. 38, 1531–1559. https://doi.org/https://doi.org/10.2134/jeq2008.0379

Pang, L., Farkas, K., Lin, S., Hewitt, J., Premaratne, A., Close, M., 2021. Attenuation and transport of human enteric viruses and bacteriophage MS2 in alluvial sand and gravel aquifer media—laboratory studies. Water Res. 196, 117051. https://doi.org/https://doi.org/10.1016/j.watres.2021.117051

Rafie, K., Lenman, A., Fuchs, J., Rajan, A., Arnberg, N., Carlson, L.A., 2021. The structure of enteric human adenovirus 41 — A leading cause of diarrhea in children. Sci. Adv. 7, eabe0974. https://doi.org/10.1126/sciadv.abe0974

Ramazanpour Esfahani, A., Batelaan, O., Hutson, J.L., Fallowfield, H.J., 2020. Combined physical, chemical and biological clogging of managed aquifer recharge and the effect of biofilm on virus transport behavior: A column study. J. Water Process Eng. 33, 101115. https://doi.org/10.1016/j.jwpe.2019.101115

Reitter, C., Petzoldt, H., Korth, A., Schwab, F., Stange, C., Hambsch, B., Tiehm, A., Lagkouvardos, I., Gescher, J., Hügler, M., 2021. Seasonal dynamics in the number and composition of coliform bacteria in drinking water reservoirs. Sci. Total Environ. 787, 147539. https://doi.org/https://doi.org/10.1016/j.scitotenv.2021.147539

Rivett, M.O., Buss, S.R., Morgan, P., Smith, J.W.N., Bemment, C.D., 2008. Nitrate attenuation in groundwater: A review of biogeochemical controlling processes. Water Res. 42, 4215–4232. https://doi.org/10.1016/J.WATRES.2008.07.020

Robinson, J., Rahmat-Samii, Y., 2004. Particle swarm optimization in electromagnetics. IEEE Trans. Antennas Propag. 52, 397–407. https://doi.org/10.1109/TAP.2004.823969

Rodríguez-Escales, P., van Breukelen, B.M., Vidal-Gavilan, G., Soler, A., Folch, A., 2014. Integrated modeling of biogeochemical reactions and associated isotope fractionations at batch scale: A tool to monitor enhanced biodenitrification applications. Chem. Geol. 365, 20–29. https://doi.org/10.1016/j.chemgeo.2013.12.003

Russian, A., Riva, M., Russo, E.R., Chiaramonte, M.A., Guadagnini, A., 2019. Stochastic inverse modeling and global sensitivity analysis to assist interpretation of drilling mud losses in fractured formations. Stoch. Environ. Res. Risk Assess. 33, 1681–1697. https://doi.org/10.1007/s00477-019-01729-4

Sadeghi, G., Behrends, T., Schijven, J.F., Hassanizadeh, S.M., 2013. Effect of dissolved calcium on the removal of bacteriophage PRD1 during soil passage: The role of double-layer interactions. J. Contam. Hydrol. 144, 78–87. https://doi.org/https://doi.org/10.1016/j.jconhyd.2012.10.006

Sasidharan, S., Bradford, S.A., Šimůnek, J., Kraemer, S.R., 2021. Virus transport from drywells under constant head conditions: A modeling study. Water Res. 197, 117040. https://doi.org/https://doi.org/10.1016/j.watres.2021.117040

Sasidharan, S., Torkzaban, S., Bradford, S.A., Cook, P.G., Gupta, V.V.S.R., 2017. Temperature

dependency of virus and nanoparticle transport and retention in saturated porous media. J. Contam. Hydrol. 196, 10–20. https://doi.org/https://doi.org/10.1016/j.jconhyd.2016.11.004

Schijven, J.F., Van den Berg, H.H.J.L., Colin, M., Dullemont, Y., Hijnen, W.A.M., Magic-Knezev, A., Oorthuizen, W.A., Wubbels, G., 2013. A mathematical model for removal of human pathogenic viruses and bacteria by slow sand filtration under variable operational conditions. Water Res. 47, 2592–2602. https://doi.org/10.1016/j.watres.2013.02.027

Schubert, J., 2002. Hydraulic aspects of riverbank filtration—field studies. J. Hydrol. 266, 145–161. https://doi.org/https://doi.org/10.1016/S0022-1694(02)00159-2

Sharma, L., Greskowiak, J., Ray, C., Eckert, P., Prommer, H., 2012. Elucidating temperature effects on seasonal variations of biogeochemical turnover rates during riverbank filtration. J. Hydrol. 428–429, 104–115. https://doi.org/https://doi.org/10.1016/j.jhydrol.2012.01.028

Sheets, R.A., Darner, R.A., Whitteberry, B.L., 2002. Lag times of bank filtration at a well field, Cincinnati, Ohio, USA. J. Hydrol. 266, 162–174. https://doi.org/https://doi.org/10.1016/S0022-1694(02)00164-6

Sprenger, C., Hartog, N., Hernández, M., Vilanova, E., Grützmacher, G., Scheibler, F., Hannappel, S., 2017. Inventory of managed aquifer recharge sites in Europe: historical development, current situation and perspectives. Hydrogeol. J. 25, 1909–1922. https://doi.org/10.1007/s10040-017-1554-8

Sprenger, C., Lorenzen, G., Grunert, A., Ronghang, M., Dizer, H., Selinka, H.-C., Girones, R., Lopez-Pila, J.M., Mittal, A.K., Szewzyk, R., 2014. Removal of indigenous coliphages and enteric viruses during riverbank filtration from highly polluted river water in Delhi (India). J. Water Health 12, 332–342. https://doi.org/10.2166/wh.2014.134

Sprenger, C., Lorenzen, G., Hülshoff, I., Grützmacher, G., Ronghang, M., Pekdeger, A., 2011. Vulnerability of bank filtration systems to climate change. Sci. Total Environ. 409, 655–663. https://doi.org/10.1016/j.scitotenv.2010.11.002

Sprinzl, M.F., Oberwinkler, H., Schaller, H., Protzer, U., 2001. Transfer of Hepatitis B Virus Genome by Adenovirus Vectors into Cultured Cells and Mice: Crossing the Species Barrier. J. Virol. 75, 5108–5118. https://doi.org/10.1128/jvi.75.11.5108-5118.2001

Stauffer, F., Bayer, P., Blum, P., Molina-Giraldo, N., Kinzelbach, W., 2013. Thermal use of shallow groundwater, Thermal Use of Shallow Groundwater. https://doi.org/10.1201/b16239

Torkzaban, S., Bradford, S.A., 2016. Critical role of surface roughness on colloid retention and release in porous media. Water Res. 88, 274–284. https://doi.org/https://doi.org/10.1016/j.watres.2015.10.022

Torkzaban, S., Hocking, M., Bradford, S.A., Tazehkand, S.S., Sasidharan, S., Šimůnek, J., 2019. Modeling Virus Transport and Removal during Storage and Recovery in Heterogeneous Aquifers. J. Hydrol. 578, 124082. https://doi.org/https://doi.org/10.1016/j.jhydrol.2019.124082

Tufenkji, N., Elimelech, M., 2004. Correlation Equation for Predicting Single-Collector Efficiency in Physicochemical Filtration in Saturated Porous Media. Environ. Sci. Technol. 38, 529–536. https://doi.org/10.1021/es034049r

Ulrich, C., Hubbard, S.S., Florsheim, J., Rosenberry, D., Borglin, S., Trotta, M., Seymour, D., 2015. Riverbed Clogging Associated with a California Riverbank Filtration System: An Assessment of Mechanisms and Monitoring Approaches. J. Hydrol. 529, 1740–1753. https://doi.org/10.1016/j.jhydrol.2015.08.012

Wang, C., Wang, R., Huo, Z., Xie, E., Dahlke, H.E., 2020. Colloid transport through soil and other

porous media under transient flow conditions—A review. WIREs Water 7, e1439. https://doi.org/https://doi.org/10.1002/wat2.1439

Wang, H., Knabe, D., Engelhardt, I., Droste, B., Rohns, H.-P., Stumpp, C., Ho, J., Griebler, C., 2022. Dynamics of pathogens and fecal indicators during riverbank filtration in times of high and low river levels. Water Res. 209, 117961. https://doi.org/https://doi.org/10.1016/j.watres.2021.117961

Weiss, W.J., Bouwer, E.J., Aboytes, R., LeChevallier, M.W., O'Melia, C.R., Le, B.T., Schwab, K.J., 2005. Riverbank filtration for control of microorganisms: Results from field monitoring. Water Res. 39, 1990–2001. https://doi.org/https://doi.org/10.1016/j.watres.2005.03.018

WHO, 2017. Guidelines for drinking-water quality, 4th edition, incorporating the 1st addendum. Geneva: World Health Organization. Geneva, Switzerland, World Health Organization.

Zhang, Y., Hubbard, S., Finsterle, S., 2011. Factors Governing Sustainable Groundwater Pumping near a River. Ground Water 49, 432–444. https://doi.org/10.1111/j.1745-6584.2010.00743.x